

## Street-scale air quality modelling for Beijing during a winter 2016 measurement campaign

Michael Biggart<sup>1</sup>, Jenny Stocker<sup>2</sup>, Ruth M. Doherty<sup>1</sup>, Oliver Wild<sup>3</sup>, Michael Hollaway<sup>3,12</sup>, David Carruthers<sup>2</sup>, Jie Li<sup>4</sup>, Qiang Zhang<sup>5</sup>, Ruili Wu<sup>5</sup>, Simone Kotthaus<sup>6,7</sup>, Sue Grimmond<sup>6</sup>, Freya A. Squires<sup>8</sup>, James Lee<sup>8,9</sup>, and Zongbo Shi<sup>10,11</sup>

<sup>1</sup>School of Geosciences, The University of Edinburgh, Edinburgh, UK

<sup>2</sup>Cambridge Environmental Research Consultants, Cambridge, UK

<sup>3</sup>Lancaster Environment Centre, Lancaster University, Lancaster, UK

<sup>4</sup>State Key Laboratory of Atmospheric Boundary Layer Physics and Atmospheric Chemistry, Institute of Atmospheric Physics, Chinese Academy of Sciences, Beijing, China

<sup>5</sup>Ministry of Education Key Laboratory for Earth System Modelling, Department of Earth System Science, Tsinghua University, Beijing, China

<sup>6</sup>Department of Meteorology, University of Reading, Reading, UK

<sup>7</sup>Institut Pierre Simon Laplace, École Polytechnique, Palaiseau, France

<sup>8</sup>Wolfson Atmospheric Chemistry Laboratories, Department of Chemistry, University of York, York, UK

<sup>9</sup>National Centre for Atmospheric Science, University of York, York, UK

<sup>10</sup>School of Geography Earth and Environmental Sciences, University of Birmingham, Birmingham, UK

<sup>11</sup>Institute of Surface-Earth System Science, Tianjin University, Tianjin, China

<sup>12</sup>Now at: Centre for Ecology & Hydrology, Lancaster Environment Centre, Bailrigg, Lancaster, UK

Correspondence to: Michael Biggart (Michael.Biggart@ed.ac.uk)

**Abstract.** We examine the street-scale variation of NO<sub>x</sub>, NO<sub>2</sub>, O<sub>3</sub> and PM<sub>2.5</sub> concentrations in Beijing during the Atmospheric Pollution and Human Health in a Chinese Megacity (APHH-China) winter measurement campaign in November - December 2016. Simulations are performed using the urban air pollution dispersion and chemistry model ADMS-Urban, and an explicit network of road source emissions. Two versions of the gridded Multi-resolution Emission Inventory for China (MEIC v1.3) are used: the standard MEIC v1.3 emissions and an optimised version, both at 3 km resolution. We construct a new traffic emissions inventory by apportioning the transport sector onto a detailed spatial road map. Agreement between mean simulated and measured pollutant concentrations from Beijing's air quality monitoring network and the Institute of Atmospheric Physics (IAP) field site is improved when using the optimised emissions inventory. The inclusion of fast NO<sub>x</sub>-O<sub>3</sub> chemistry and explicit traffic emissions enables the sharp concentration gradients adjacent to major roads to be resolved with the model. However, NO<sub>2</sub> concentrations are overestimated close to roads, likely due to the assumption of uniform traffic activity across the study domain. Differences between measured and simulated diurnal NO<sub>2</sub> cycles suggest that an additional evening NO<sub>x</sub> emission source, likely related to heavy duty diesel trucks, is not fully accounted for in the emissions inventory. Overestimates in simulated early evening NO<sub>2</sub> are reduced by delaying the formation of stable boundary layer conditions in the model to replicate Beijing's urban heat island. The simulated campaign period mean PM<sub>2.5</sub> concentration range across the monitoring network (~15 µg m<sup>-3</sup>) is much lower than the measured range (~40 µg m<sup>-3</sup>). This is likely a consequence of insufficient PM<sub>2.5</sub> emissions and spatial variability, neglect of explicit point sources, and assumption of a homogeneous background PM<sub>2.5</sub> level. Sensitivity studies highlight that the use of explicit road source emissions, modified diurnal emission profiles, and inclusion of urban heat island effects permit closer agreement between simulated and measured NO<sub>2</sub> concentrations. This work lays the foundations for future studies of human exposure to ambient air pollution across complex urban areas, with the APHH-China campaign measurements providing a valuable means of evaluating the impact of key processes on street-scale air quality.

## 1 Introduction

In recent decades, China's rapid economic growth, industrialisation and urbanisation has led to severely deteriorating air quality. Associations between high concentrations of air pollutant species, such as fine particulate matter (PM<sub>2.5</sub>), nitrogen oxides (NO<sub>x</sub> = NO + NO<sub>2</sub>) and ozone (O<sub>3</sub>), and adverse health effects are well-established in China (Han et al. 2018). Most notably, the inhalation of ambient PM<sub>2.5</sub> is linked to respiratory illnesses, cardiovascular disease, lung cancer and adverse birth outcomes (Han et al. 2018; Liang et al. 2019). The Global Burden of Disease Study 2016 identified ambient PM<sub>2.5</sub> exposure as the fourth leading cause of premature death in China (GBD 2016 Risk Factors Collaborators, 2017).

To accurately assess the extent of human exposure to pollution in densely populated and complex urban areas and to reduce this health risk, comprehensive information is needed on the spatiotemporal variation of ambient pollutant concentrations, the dominant emission source sectors, chemical processes and the role of meteorological conditions in pollution accumulation and dispersion. High quality air pollutant concentration measurements can provide some of the required information. For instance in Beijing, a 35 station automated air quality monitoring network has measured continuous hourly concentrations of PM<sub>2.5</sub>, PM<sub>10</sub>, SO<sub>2</sub>, NO<sub>2</sub>, O<sub>3</sub> and CO since 2013. However, these measurements, recorded by Beijing's Environment Protection Bureau (EPB), are sparsely distributed (Chen et al. 2015; Li et al. 2018; Cui et al. 2019; Cheng et al. 2018). This, coupled with the sharp pollutant concentration gradients that exist across urban areas (Hood et al. 2018), limits the accuracy of any subsequent human exposure analyses. Therefore, air quality modelling, evaluated using network measurements, may fill in the gaps to provide complete spatially and temporally resolved concentration fields (Bates et al. 2018).

Air quality modelling, from global to street-scale, requires detailed representations of local and regional emission fields. However, generating accurate and up-to-date emissions data is a considerable challenge, owing to difficulties in obtaining the necessary activity, emission factor, and production/control technology data for each emission source sector (including power, industry, transport, residential or agriculture) (Hong et al. 2017; Qi et al. 2017). Additionally, in China, the rapid decrease in emissions of major air pollutants over recent years needs to be accounted for (Sun et al. 2018; Zheng et al. 2018). This reduction in emissions has followed the nationwide implementation of a number of clean air policies since 2013 as part of the Air Pollution Prevention and Control Action Plan (APPCAP) and more locally through the Beijing Action Plan (Cheng et al. 2018; Ni et al. 2018; Cheng et al. 2019; Wang et al. 2019). Overall, emissions in Beijing of SO<sub>2</sub>, NO<sub>x</sub>, VOCs and PM<sub>2.5</sub> are reported to have reduced by 84, 43, 42 and 55% between 2013 and 2017 (Cheng et al. 2019). These emission reductions were estimated by Cheng et al. (2019), using the technology-based model framework of the Multi-resolution Emission Inventory for China (MEIC), and are in good agreement with independent satellite-derived emission trends (Liu et al. 2016; Liu et al. 2017).

The MEIC emission inventory is widely used in studies aimed at understanding the key emission sources and the effectiveness of air pollution control measures across various regions of China (Li et al. 2017; Cheng et al. 2018; Zheng et al. 2018; Cheng et al. 2019). However, uncertainties in MEIC emissions estimates, related to its underlying methodology and input data, have also been highlighted. For instance, the MEIC model relies on the use of national and provincial energy consumption statistics, which were shown by Hong et al. (2017) to contain large sources of error. The MEIC model uses spatial proxies, such as Gross Domestic Product (GDP) and urban population density, to downscale emissions from provincial to county and grid level scale (Qi et al. 2017). A study by Zheng et al. (2017) revealed a tendency to over-allocate emissions to central urban areas when using these spatial proxies to produce the MEIC inventory at resolutions finer than 0.25°. Zheng et al. (2017) attributed this to the displacement of large industrial facilities away from urban centres, therefore decoupling the real-world location of the emissions from the population-related proxies used to represent them in the MEIC inventory.

Numerous regional modelling studies, incorporating emission inventories such as MEIC and Eulerian chemical transport models (CTMs), have been carried out for Beijing (Liu et al. 2016; Petaja et al. 2016; Li et al. 2017; Wang et al. 2017; Wang et al. 2018; Chang et al. 2019). Eulerian chemical transport models (CTMs) such as the Nested Air

85 Quality Prediction and Modeling System (NAQPMS), the Comprehensive Air Quality Model with Extensions (CAMx), and  
the joint Weather Research and Forecast—Community Multi-scale Air Quality models (WRF-CMAQ), have been used to  
investigate the relative contributions of local and regional emissions to PM<sub>2.5</sub> concentrations during severe haze periods (Li et  
al. 2017; Wang et al. 2017; Chang et al. 2019). The WRF-CMAQ model was used by Cheng et al. (2018) to deduce the relative  
90 roles of local and regional emission controls, and favourable meteorological conditions in reducing PM<sub>2.5</sub> concentrations in  
Beijing. Further CTM applications have included the assessment of different emission inventory performance as well as the  
investigation of aerosol-radiative feedback impacts on boundary layer stability and the rate of PM<sub>2.5</sub> accumulation during heavy  
haze events (Liu et al. 2016; Petaja et al. 2016; Wang et al. 2018).

A key limitation of regional models, however, is that they cannot be used to represent pollutant concentrations at the scale  
needed to fully assess human health impacts. As a result, a range of street-scale resolution air quality modelling techniques  
95 have recently emerged. Land use regression (LUR) modelling studies, combining geospatial indicators with air quality  
measurement data, can generate local scale (<1 km) pollutant level variations, but have been limited by the sparsity of  
monitoring network data available in Beijing (J. Xu et al. 2019; M. Xu et al. 2019). Alternatively, box models, such as The  
Model of Urban Network of Intersecting Canyons and Highways (MUNICH), are used to calculate pollutant concentrations  
within street canyons across street networks, but require detailed information on the spatial dimensions of a city's street canyons  
100 and are restricted by assumptions of equal in- and outfluxes of pollution within street canyons as well as uniform  
concentrations along individual road segments (Lugon et al. 2019). Gaussian plume dispersion models, capable of  
simulating dispersion from an array of explicitly represented emission source types, including road and point sources,  
are instead often implemented. Widely used for environmental regulatory purposes, models such as ADMS-Urban (Owen  
et al. 2000) and AERMOD (Cimorelli et al. 2005) incorporate detailed boundary layer parameterisations and transport processes.  
105 The additional modelling of local fast chemistry processes on pollutant emissions with ADMS-Urban, involving the  
simplified Generic Reaction Set (GRS) chemistry scheme, including NO<sub>x</sub>-O<sub>3</sub> reactions, enables sharp concentration  
gradients adjacent to major urban sources to be captured (Hood et al. 2018). Previous applications of ADMS-Urban in  
China have largely focussed on evaluating the impact that emission control schemes targeting individual sources have on  
the immediate environment. For instance, Chen et al. (2009) combined pollutant concentrations simulated by ADMS-Urban  
110 with population data to investigate the impact of traffic control policies on human exposure levels in Shanghai.  
Similarly, Cai and Xie (2011) used the ADMS-Urban model to quantify the effect that the odd-even traffic scheme  
(restricting vehicles with odd or even number plates), enforced during the 2008 Olympics, had on emissions from a  
selection of major roads, finding that some of the previously most polluted areas subsequently complied with the  
Chinese National Air Quality Standards (CNAAQs).

This study aims to produce, for the first time, fully resolved street-scale NO<sub>2</sub>, O<sub>3</sub> and PM<sub>2.5</sub> concentrations across  
115 urban and suburban Beijing using ADMS-Urban and explicit source road traffic emissions. Previously, Yang et al. (2019)  
used the RapidAir dispersion model in Beijing, which excludes chemical processes, and a link-level traffic emissions  
inventory developed using congestion maps and manual vehicle counts to simulate pollutant concentrations at the street  
level. A bottom-up street-scale vehicle emissions inventory was also created by Zhang et al. (2018), using traffic  
surveys and video identification of vehicle fleet composition, to evaluate the impact of a new low emission zone  
(LEZ) in urban Beijing. For this study, we compile an explicit source traffic emissions inventory by apportioning  
120 gridded emissions onto the freely available OpenStreetMap (OSM) road network geometry. Unlike the data-  
intensive methodologies adopted by Zhang et al. (2018) and Yang et al. (2019), spatiotemporal variations in  
traffic volume and vehicle type are not considered here. However, this work provides a robust framework suitable  
for similar street-scale air quality modelling across large urban areas in cities with limited data availability that  
future human health studies can build on. Furthermore, both the MEIC v1.3 and an optimised version of the  
125 same inventory are used to assess the performance of proxy-based inventories for street-scale modelling.  
Aggregated sectoral emissions (industrial, power and residential) are also included. Simulations are performed  
We perform simulations for the Atmospheric Pollution and Human Health in a Chinese megacity (APHH-China) winter  
measurement

Formatted: Indent: First line: 0 cm

130 campaign period, which took place in November-December 2016 at the Institute of Atmospheric Physics (IAP), Chinese  
Academy of Sciences (Shi et al. 2019). [Measured pollutant concentrations from both the APHH-China campaign and Beijing's  
135 air quality monitoring network are used to evaluate modelled concentrations, providing valuable insight into the key processes  
that impact street-scale air quality.](#) The adaptability of ADMS-urban is utilised in a series of further sensitivity simulations  
aimed at exploring the impact that explicit road traffic emissions, modified diurnal emissions profiles and Beijing's evening  
urban heat island (UHI) have on discrepancies between measured and modelled pollutant concentrations.

135 A detailed description of the ADMS-Urban model and its inputs is provided in Sect. 2. Section 3 presents an  
evaluation and discussion of results comparing modelled concentrations, using both emission inventories, with monitoring  
network and field campaign measurement data. A summary of this work's primary findings is provided in Sect. 4 along with  
details of possible future study development.

140 Hence, Gaussian plume dispersion models, capable of simulating pollutant dispersion from explicitly represented  
emission sources, are often implemented. Widely used for environmental regulatory purposes, models such as ADMS-Urban  
(Owen et al. 2000) and AERMOD (Cimorelli et al. 2005) incorporate detailed transport processes and simplified fast chemistry  
schemes, commonly including  $\text{NO}_x$ - $\text{O}_3$  reactions, enabling the sharp concentration gradients adjacent to major urban sources  
to be captured (Hood et al. 2018). Modelling studies, with ADMS-Urban, have been performed at various degrees of  
145 complexity, in terms of emission sources represented, in a number of cities globally. For example, Munir and Habeebullah  
(2018) investigated roadside  $\text{PM}_{2.5}$  and  $\text{PM}_{10}$  levels in Makkah, Saudi Arabia, using only a bottom-up road traffic emissions  
inventory and Dédélé and Miskinyte (2015) simulated  $\text{NO}_2$  concentrations in Kaunas City, Lithuania, using transport, industrial  
and residential sector emissions but excluded buildings information. Hood et al. (2018) incorporated traffic emissions  
adjustments to account for differences between real-world and test driving cycles, as well as comprehensive 3-D buildings  
data, to evaluate the performance of ADMS-Urban across London, UK.

150 In China, applications of ADMS-Urban have focussed on evaluating the impact that emission control  
schemes targeting individual sources have on the immediate environment. For instance, Chen et al. (2009) combined pollutant  
concentrations simulated by ADMS-Urban with population data to investigate the impact of traffic control policies on human  
exposure levels in Shanghai. Similarly, Cai and Xie (2011) used the ADMS-Urban model to quantify the effect that the odd-  
even traffic scheme (restricting vehicles with odd or even number plates), enforced during the 2008 Olympics, had on  
155 emissions from a selection of major roads, finding that some of the previously most polluted areas subsequently complied with  
the Chinese National Air Quality Standards (CNAAQs).

This study aims to produce, for the first time, fully resolved street-scale  $\text{NO}_2$ ,  $\text{O}_3$  and  $\text{PM}_{2.5}$  concentrations across  
urban and suburban Beijing using ADMS-Urban and explicit source road traffic emissions. Compiling the traffic emissions  
inventory involves apportioning gridded emissions onto the freely available OpenStreetMap (OSM) road network geometry.  
This approach is much less data-intensive than alternative vehicle activity-based bottom-up methodologies such as the link-  
160 level traffic emissions inventory developed for Beijing by Yang et al. (2019) using congestion maps and manual vehicle counts.  
Both the MEIC v1.3 and an optimised version of the same inventory are used to assess the performance of proxy-based  
inventories for street-scale modelling. Aggregated sectoral emissions (industrial, power and residential) are also included.  
Simulations are performed for the Atmospheric Pollution and Human Health in a Chinese megacity (APHH-China) winter  
measurement campaign period, which took place in November-December 2016 at the Institute of Atmospheric Physics (IAP),  
165 Chinese Academy of Sciences (Shi et al. 2019).

A detailed description of the ADMS-Urban model and its inputs is provided in Sect. 2. Section 3 presents an  
evaluation and discussion of results comparing modelled concentrations, using both emission inventories, with monitoring  
network and field campaign measurement data. Sensitivity studies are included to explore the impact that explicit road traffic  
emissions, modified diurnal emissions profiles and Beijing's evening urban heat island (UHI) have on measured and simulated

170 pollutant concentration agreement. A summary of this work's primary findings is provided in Sect. 4 along with details of  
possible future study development.

## 62 Methodology

The street-scale air pollution dispersion and chemistry model, ADMS-Urban, is used here to simulate ambient concentrations  
of  $\text{NO}_x$ ,  $\text{NO}_2$ ,  $\text{O}_3$  and  $\text{PM}_{2.5}$  across Beijing during the APHH-China winter campaign period (5 November 2016 – 10 December  
175 2016). Section 2.1 provides a full description of the model and its configuration for Beijing, including details on emission  
source types, pollution dispersion, chemical processes and background pollutant concentrations. Emission inventory  
development, including the construction of an explicit network of road source emissions, is outlined in Sect. 2.2. In Section  
2.3, the statistical measures used to evaluate model performance are described.

### 2.1 Model Description and Set-up

180 ADMS-Urban, developed by Cambridge Environmental Research Consultants (CERC), is a quasi-Gaussian pollution  
dispersion and chemistry model that has been applied worldwide for environmental regulation (McHugh et al. 2005),  
investigation and assessment of emission control strategies (Cai and Xie, 2011) and generation of high spatial resolution air  
quality forecasts (McHugh et al. 2005; Carruthers, 2009; Cai and Xie, 2011).

The model domain (75 km x 90 km) covers urban Beijing, defined here as everywhere within the Sixth Ring Road  
185 (marked in Fig. 1), and extends into the suburban counties of Shunyi and Changping to the north and Tongzhou, Daxing and  
Fangshan to the south, as illustrated by Fig. 1.

#### 2.1.1 Emission sources, meteorological inputs and surface parameters

In the model, pollutant emissions are represented as individual plumes dispersing from a range of explicitly represented sources,  
including point, road, area and volume sources. Aggregate grid sources (2-D and 3-D) are used to account for additional,  
190 poorly-defined diffuse emissions (e.g domestic heating or minor roads) (Mohan et al. 2011; Dédelé and Miskinyté, 2015; Hood  
et al. 2018). Plume dispersion calculations are driven by a single set of ~~hourly~~ meteorological measurements that are  
representative of upwind conditions and assumed to be homogeneous across the study domain. For this study, we use ~~hourly~~  
wind speed, ~~wind direction and direction~~, air temperature and cloud cover data from the Beijing Capital International Airport  
Meteorology Observatory, which is located ~20 km northeast of the Fourth Ring Road (Fig. 1). The input meteorology is  
195 processed by the model to calculate parameters that determine the stability and height of the planetary boundary layer (PBL)  
for each hour. Cloud cover measurements, along with the time of day and day of year, are used to calculate incoming solar  
radiation which generates surface sensible heat flux ( $F_{00}$ ), friction velocity ( $U^*$ ) and Monin-Obukhov length ( $L_{MO}$ ) terms via  
the surface energy balance.  $L_{MO}$  is a measure of the relative importance of mechanical turbulence and buoyancy in the PBL  
and along with surface heat flux terms determines PBL height (PBLH) in the model. Alternatively, measurements of PBLH  
200 can be used if available. For this study, simulations are performed using directly input observations of mixed layer height  
(MLH) derived from ceilometer measurements taken at the IAP field site during the APHH-China campaign (Kotthaus et al.  
2016; Shi et al. 2019). The MLH represents the height of the lowest atmospheric layer always in direct contact with the earth's  
surface resulting from turbulent exchange (Kotthaus and Grimmond, 2018) and is assumed here to equate to the model's PBLH  
output.

205 ADMS-Urban calculates the ratio of PBLH to  $L_{MO}$ , a measure of the relative importance of mechanical turbulence  
and buoyancy, to generate a continuous PBL stability profile that varies with height. This PBLH/ $L_{MO}$  parameterisation controls  
the ~~subsequently generated~~ vertical and horizontal plume-spread extents of each emitted Gaussian plume, with the aggregate

contribution from each individual emission source determining hourly simulated pollutant concentrations. In unstable conditions, an additional convectively driven turbulence component is calculated. This produces a skewed, non-Gaussian concentration distribution, meaning that for elevated sources the height of maximum concentration and mean height of the plume itself will descend and ascend, respectively (CERC, 2017).

Differences between conditions at the exposed airport meteorological site and the predominantly built-up modelling domain, largely caused by frictional effects of buildings and street canyons that perturb near-surface dynamics locally, are accounted for through distinct definitions of surface roughness ( $Z_0$ ) and minimum Monin-Obukhov length ( $L_{MO}$ ) in both environments.  $Z_0$  and minimum  $L_{MO}$  values of 0.5 m and 30 m, respectively, represent conditions at the meteorological measurement site. However, greater  $Z_0$  and minimum  $L_{MO}$  values of 1.5 m and 100 m, respectively, typical of urban areas dominated by densely packed tall buildings and concrete surfaces (Stewart and Oke, 2012), are used across the modelling domain and displace the upwind vertical wind speed, wind direction and turbulence profiles derived from the meteorological measurements.

#### 6.1.22.1.2 PBL stability adjustment

Both  $Z_0$  and minimum  $L_{MO}$  definitions prevent the modelled boundary layer from becoming unrealistically stable in urban areas where the surface radiation balance is perturbed by a number of factors including anthropogenic heat release, building geometry and the thermal properties of concrete surfaces (Oke, 1982). The resulting positive temperature differential between urban areas and the surrounding rural environment is referred to as the urban heat island (UHI) effect (Hamilton et al. 2014). This phenomenon is strongest in the late afternoon and early evening hours, when anthropogenic heat from rush hour traffic and residential heating systems, as well as incoming solar radiation stored in the urban fabric throughout the day, is released into a stabilising PBL (Liu et al. 2007).

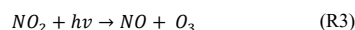
For this study, a further restriction on PBL stability has been applied to more comprehensively account for Beijing's strong evening UHI (Wang et al. 2017). Figure 2 shows how the PBL stability, represented by  $PBLH/L_{MO}$ , varies diurnally for the campaign period. The  $L_{MO}$  values are derived from a prior model simulation without stability modifications and the observed MLH (Sect. 2.2.1) is used as the PBLH.  $PBLH/L_{MO} > 1$ ,  $-0.3 \leq PBLH/L_{MO} \leq 1$  and  $PBLH/L_{MO} < -0.3$  represent stable, neutral and unstable conditions, respectively.

During the day, the surface net radiation is partitioned between upwards fluxes of sensible and latent heat and the downwards flux of heat into the ground (Oke, 1982). The version of ADMS-Urban used here (v 4.2) assumes that this ground heat flux is a constant proportion of the net radiation. In reality, this proportion varies diurnally, peaking around midday when a greater proportion of incoming solar radiation is stored by the urban fabric (Anandakumar, 1999; Grimmond and Oke, 1999). The release of this excess heat in the early evening sustains convection in the PBL, prolonging its instability. ~~To account for this, a constant rate of decrease of  $PBLH/L_{MO}$  has been assumed between original modelled values for 3 pm and 8 pm, producing the modified campaign period mean  $PBLH/L_{MO}$  diurnal profile illustrated in Fig. 2. Modified  $L_{MO}$  values from 4-7 pm are added to the set of input meteorological variables for all subsequent simulations, with the directly input PBLH measurements remaining unchanged.~~ To account for this, a constant rate of decrease of  $PBLH/L_{MO}$  has been assumed between original modelled values for 3 pm and 8 pm, producing the modified campaign period mean  $PBLH/L_{MO}$  diurnal profile illustrated in Fig. 2. Modified  $L_{MO}$  values from 4-7 pm are added to the set of input meteorological variables for all subsequent simulations, with the directly input PBLH measurements remaining unchanged. This adjustment increases sensible and latent heat fluxes, therefore enhancing the turbulent mixing of air during this early evening period. The 4-7 pm time window is chosen as it coincides with sunset in November-December in Beijing and it is in agreement with the extended duration of evening sensible heat flux decay in urban areas, compared with surrounding rural areas, observed by other UHI-related studies (Zhou et al. 2013; Barlow et al. 2015). Without this adjustment, the model tends to predict overly stable meteorological conditions in the early evening, which can lead to the over-prediction of pollutant concentrations. It is important to note that

250 the modelled surface heat flux and  $L_{MO}$  terms are calculated independently of the PBLH, so that small positive  $L_{MO}$  values can generate an overly stable boundary layer even when paired with the measured MLH assumed here to represent real-world stability conditions.

### 6.1.32.1.3 Chemistry

255 The chemical transformation of pollutants contained within each dispersing plume is represented using the Generic Reaction Set (GRS) chemistry scheme (Malkin et al. 2016). Typically, regional CTMs such as WRF-Chem and CMAQ use detailed chemical mechanisms containing hundreds, or even thousands of reactions involving NO, NO<sub>2</sub>, O<sub>3</sub> and VOCs, including homogeneous and heterogeneous aerosol production (Sarwar and Luecken, 2008). The GRS, however, simplifies these to the following seven reactions:



where ROC represents Reactive Organic Compounds, RP is the Radical Pool, SGN is the Stable Gaseous Nitrogen product and SNGN is the Stable Non-Gaseous Nitrogen product (CERC, 2017). The inclusion of fast NO<sub>x</sub>-O<sub>3</sub> chemistry, whereby 270 high NO<sub>x</sub> levels, NO consumes O<sub>3</sub> (R3 and R4), enables the sharp pollutant species concentration increases, with proximity to major road or large point sources, to be captured. R1 summarises all of the oxidation and photolysis reactions that lead to radical production from VOCs (Malkin et al. 2016), while R2 and R5 represent subsequent radical loss.

275 An additional set of reactions involves the production of ammonium sulphate, following the oxidation of SO<sub>2</sub> and reactions with water and ammonia, and this provides a source of both PM<sub>10</sub> and PM<sub>2.5</sub>. Other secondary organic and inorganic components of particulate matter, which can comprise up to a combined 70% of total PM<sub>2.5</sub> mass in Beijing (Ma et al. 2014; Tao et al. 2017; Wang et al. 2017), are accounted for in the background concentration field described in Sect. 2.1.4.

### 6.1.42.1.4 Background pollutant concentrations

280 Background pollutant concentrations represent the regional pollution levels on which the local emissions build. For this study, background levels for NO<sub>2</sub>, O<sub>3</sub>, PM<sub>2.5</sub>, PM<sub>10</sub>, SO<sub>2</sub> and CO are derived directly from hourly air quality measurement data [and provided by the China National Environmental Monitoring Center \(CNEMC\)](#) and are assumed to be uniform across the study domain. Measured concentrations at 12 [national air quality monitoring stations, run by the China National Environmental Monitoring Center \(CNEMC\), of the 35 monitoring stations comprising Beijing's administrative air pollution monitoring network](#), the IAP field site and an additional site 60 km SE of Beijing, situated in the built-up Guangyang district of Langfang in Hebei province, are used to estimate this background concentration field. The locations of these 14 sites are given in Table 1.

285 1.

290 For particulate matter (PM<sub>2.5</sub> and PM<sub>10</sub>), an hourly upwind background concentration is derived [based on wind direction with concentrations selected from using sites 3 \(270-360°\), 10 \(0-90°\) and 14 \(90-270°\) three sites](#) located to the NW, NE and SE of urban Beijing, [respectively with concentrations selected based on wind direction](#). Particulates have near-surface lifetimes of days to weeks, therefore concentrations in Beijing are heavily influenced by long-range transport (LRT) of both primary and secondary components originating in neighbouring industrial regions (Wang et al. 2017; Cheng et al. 2019<sup>8</sup>). The measured upwind concentration is expected to capture this transported background regional air. Gaseous species such as NO<sub>2</sub>, have a much shorter lifetime (~ 1 day) and therefore a smaller regional contribution, with concentrations across urban areas dominated primarily by local traffic sources (Zhang et al. 2014). The NO<sub>2</sub> concentrations at the upwind monitoring station were subsequently not deemed representative of the true background value owing to both this greater spatial variation and the proximity of the upwind monitoring stations to local emission sources. Instead, to approximate background values for gaseous species (NO<sub>2</sub>, O<sub>3</sub>, CO and SO<sub>2</sub>), the hourly minimum concentration for each pollutant across the 12 network monitoring stations and the IAP field site is selected, yielding an approximation for the underlying conditions uninfluenced by local sources.

### 6.22.2 Emissions inventory processing

300 For this study, ADMS-Urban simulations use both aggregate 3-D grid source and explicit road source emissions of NO<sub>x</sub>, NO<sub>2</sub>, SO<sub>2</sub>, VOC (total), PM<sub>2.5</sub>, PM<sub>10</sub> and CO derived from a standard and an optimised version of the high-resolution (3 km) MEIC v1.3 emissions inventory. The standard MEIC v1.3 emissions inventory, for 2013, consists of five emission source sectors: transportation, power, industrial, residential and agricultural (Qi et al. 2017). Note that the latter is not used in this study [due to both the lack of farmland in urban Beijing and the negligible contributions to the pollutant species simulated in this study from agricultural emission sources](#) (Qi et al. 2017). The transportation sector is estimated following Zheng et al. (2014), in which county-level emissions, derived from county-level vehicle ownership, are downscaled to grids based on road network and road-specific vehicle activity data. Liu et al. (2015) describes the unit-based technique, adopted to generate the power sector emissions, which utilises the Coal-fired Power Plant Emissions Database (CPED), including information on the technologies, activity data, operation situation, emission factors and locations of individual units. [Industrial and residential sector emissions are calculated from provincial level activity data and emission factors](#) (Zheng et al. 2017). [Industrial emissions are downscaled to the county level using GDP \(National Bureau of Statistics, 2014\), with both industry and residential emissions further distributed to grid level resolutions based on high resolution \(~ 1 km\) population density data \(Oak Ridge National Laboratory, 2013\) \(Zheng et al. 2017\).](#) [The industrial and residential sectors are both calculated with provincial level activity rates and emission factors before downscaling to county and grid level resolutions based on Gross Domestic Product \(GDP\) and population density distribution \(Zheng et al. 2017\).](#) To model conditions during the APHH-China winter campaign, the MEIC v1.3 emissions inventory is re-scaled for this study to account for the 2013-2016 emission reductions in Beijing (Sect. 1). According to Cheng et al. (2019<sup>8</sup>), total emissions of NO<sub>x</sub> (and NO<sub>2</sub>), SO<sub>2</sub>, VOCs and PM (PM<sub>2.5</sub> and PM<sub>10</sub>) in Beijing were estimated to reduce by 30, 63, 27, 35 and 30%, respectively, between 2013 and 2016. This adjusted MEIC v1.3 emissions inventory is hereafter referred to as MEIC Std.

310  
315  
320 An alternate optimised version of MEIC v1.3 (hereafter referred to as MEIC Opt) was created (Li et al. 2018), for November and December 2016, with the aim of addressing the over-allocation of emissions to urban areas that occurs when downscaling MEIC v1.3 to fine scales based on proxy data (Zheng et al. 2017). This MEIC Opt inventory was created using the Nested Air Quality Prediction Modeling System (NAQPMS) to perform iterative minimisation of a cost function comparing NAQPMS simulations with winter campaign observations (Li et al. 2018). This optimisation algorithm was used to redistribute MEIC emissions from central urban Beijing to suburban and rural areas, and to adjust their magnitude to represent the campaign period. Both MEIC Std and MEIC Opt inventories comprise of monthly varying emissions with distinct diurnal weighting profiles applied to each emission sector.

Aggregate 3-D grid sources contain the sum of all MEIC emission source sectors (residential, transportation, industrial and power) and consist of seven vertical layers (38, 90, 152, 228, 337, 480 and 660 m). In the absence of sufficient information required to model point source emissions (e.g large power plants) explicitly, ADMS-Urban's 3-D grid sources enable plume release and dispersion from each of the seven grid source heights, accounting for tall emission sources included within the MEIC v1.3 power or industrial sector grids. MEIC Std and MEIC Opt campaign period mean NO<sub>2</sub>, NO<sub>x</sub>, PM<sub>2.5</sub>, PM<sub>10</sub>, SO<sub>2</sub> and VOC emission rates from 3-D grid sources, aggregated across all, urban and suburban grid cells, are shown in Table 2.

An explicit network of road emissions for Beijing has been constructed based on the MEIC transportation sector emissions. Figure 3 illustrates the pseudo-top down approach adopted here in the absence of detailed information on traffic activity and fleet composition. Figure 3a shows the spatial distribution of the November and December mean MEIC Std transportation sector surface NO<sub>2</sub> emissions. The transportation sector emissions of all pollutants are apportioned to individual road segments on a grid cell-by-grid cell basis, using the geographic information system software ArcGIS. The spatial road network of Beijing, presented in Fig. 3b, is provided by the OpenStreetMap dataset (<https://openstreetmap.org/>) and includes individual road segment type and geometry information. Emissions are mapped onto the road network based on each road segment length and an emissions weighting factor, producing the distribution shown in Fig. 3c, following Eq. (1):

$$E_{mis_{i,j,k}} = \frac{l_{i,j} \cdot w_k}{\sum_{i=1}^n (l_{i,j} \cdot w_k)} \times E_j \quad (1)$$

where  $l_{i,j}$  represents the length of road segment  $i$  in grid cell  $j$  of road type  $k$ . The weighting factor of road type  $k$  is given by  $w_k$ .  $E_j$  and  $n$  denote the total traffic emissions and number of road segments in grid cell  $j$ , respectively. A weighted mean emission rate, based on road segment length, is calculated along segments traversing multiple grid cells in order to avoid discontinuities.

Weighting factors (Table 3) are estimated using road type and width (based on manual inspection of the most frequent number of lanes for each road type), acting as proxies for traffic activity. [Each road type weighting factor is applied equally to all pollutant species.](#) The magnitude of weighting factors relative to each other is important, rather than their absolute values, according to Eq. (1). Minor roads were removed from the network to limit the computational expense of each simulation and are instead aggregated within the 3-D grid sources. This methodology is based on the assumption that traffic volume, speed and fleet composition and behaviour are constant across all road type classes listed in Table 3. However, substantial variations in traffic flow characteristics on roads of the same classification within Beijing's urban area have been observed. For example, Jing et al. (2016) used GPS-fitted buses and taxis to collect near real-time traffic data along the major road types in Beijing, finding much greater levels of congestion closer to the urban centre, causing increased traffic volume and vehicle speed variations. [Additionally, Zhang et al. \(2018\) observed a greater proportion of vehicles with lower emission standards on roads outside the Fifth Ring Road.](#) Given that the same emission weighting factors for roads of the same class are applied across the domain and the lack of traffic flow variations on specific roads within cities in the MEIC framework (Zheng et al. 2014), the methodology adopted here may under-allocate emissions on more congested inner-city roads and over-allocate emissions in suburban areas.

### 6.3.2.3 Model evaluation

Evaluation of regional-scale Eulerian CTMs involves the comparison of measurements at specific monitoring site locations with simulated concentrations in the nearest model grid box (Zhong et al. 2016; Wang et al. 2017; Zheng et al. 2017). However, for street-scale air quality modelling with ADMS-Urban, pollutant concentrations can be simulated at specific locations, referred to hereafter as receptor points. For this study, concentrations are modelled at the locations of the 12 monitoring network stations, as well as the IAP field site, for direct comparison with the corresponding measured concentrations. The

following three statistical performance measures are considered simultaneously enabling a comprehensive evaluation of modelled predictions of concentrations, using both MEIC Std and MEIC Opt emissions inventories, during the APHH-China winter campaign period:

$$\text{Normalised mean square error (NMSE)} = \frac{\overline{(M - O)^2}}{\overline{MO}} \quad (2)$$

$$\text{Fractional bias (Fb)} = \frac{\overline{M} - \overline{O}}{0.5(\overline{O} + \overline{M})} \quad (3)$$

$$\begin{aligned} \text{Pearson's correlation coefficient (R)} \\ = \frac{1}{n-1} \sum_{i=1}^n (M_i - \overline{M}/\sigma_M) (O_i - \overline{O}/\sigma_O) \end{aligned} \quad (4)$$

370

375 where  $n$  denotes the total number of matching hourly modelled and observed concentrations;  $\overline{M}$  and  $\overline{O}$  indicate mean modelled and observed concentrations, respectively, and  $\sigma$  is the standard deviation.

NMSE (ideal value = 0) is a measure of the model's overall accuracy (Cai and Xie, 2011), incorporating the effects of both systematic and random errors (Patryl and Galeriu, 2011); Fb (ideal value = 0) reflects the model's tendency to overestimate or underestimate concentrations, compared to measurements; and R (ideal value = 1) informs on the extent to which modelled and measured values are linearly related.

380

[In this study, the statistical evaluation of pollutant concentrations simulated at the exact coordinates of the measurement locations is complemented by street-scale resolution maps which more clearly illustrate the strong spatial heterogeneity of pollution levels across Beijing. Fully resolved PM<sub>2.5</sub>, NO<sub>2</sub> and O<sub>3</sub> concentration fields in central Beijing are simulated with a combination of regularly spaced receptor points at ~150 m and additional output points distributed within and in the immediate vicinity of all individual road emission source segments. The addition of emission source-oriented output points increases the model resolution to < 10 m across regions containing dense distributions of explicit road sources, therefore enabling the sharp pollutant concentration variations adjacent to roads to be captured.](#)

385

### 7.3 Results and Discussion

390 Street-scale resolution maps of PM<sub>2.5</sub>, NO<sub>2</sub> and O<sub>3</sub> concentrations across a region of urban Beijing are presented in Sect. 3.1. Section 3.2 provides a statistical evaluation of simulated pollutant species against hourly measurements at 12 monitoring network sites and the IAP campaign field site (Table 1), using both MEIC Std and MEIC Opt inventories. Diurnal cycles of NO<sub>x</sub>, NO<sub>2</sub> and O<sub>3</sub> concentrations are given in Sect. 3.3, and Sect. 3.4 contains an analysis of local and regional PM<sub>2.5</sub> sources. Sensitivity studies explore the impact on model performance of including explicit road emission sources, varying diurnal emissions profiles and accounting for the evening UHI in Sect. 3.5, 3.6 and 3.7, respectively.

395

#### 3.1 Street-scale variation of PM<sub>2.5</sub>, NO<sub>2</sub> and O<sub>3</sub> concentrations

Mean PM<sub>2.5</sub>, NO<sub>2</sub> and O<sub>3</sub> concentrations simulated for the campaign period (5 November-10 December 2016), using the MEIC Opt inventory, for a region of urban Beijing within the Fifth Ring Road are presented in Fig. 4. The influence of the explicit road emissions network on the spatial variation of all species is clear, most notably along the Second, Third and Fourth Ring Roads. PM<sub>2.5</sub> and NO<sub>2</sub> concentrations peak at 125 µg m<sup>-3</sup> and 160 µg m<sup>-3</sup>, respectively, along the ring road centrelines, before

400

sharply decaying. The magnitude of this drop and distance across which it occurs is determined not only by emission source strength but also by physical and chemical mechanisms, with the speed of plume dispersion and mixing, controlled by mechanical and convective turbulence generation, interacting with the differing lifetimes of individual pollutants. In Fig. 5, mean NO<sub>2</sub> concentrations reduce by ~20-25 μg m<sup>-3</sup> along a horizontal profile extending 100 m either side of the Second Ring Road. The spatial variation of O<sub>3</sub> concentrations is approximately inversely related to these NO<sub>2</sub> levels. Modelled O<sub>3</sub> concentrations reduce to 5 μg m<sup>-3</sup> along the Second Ring Road centreline and reach 25 μg m<sup>-3</sup> between the Fourth and Fifth Ring Roads (Fig. 4). This is a result of the fast reaction of O<sub>3</sub> with NO (titration) (R4) which dominates in high NO<sub>x</sub> environments (Zhang et al. 2015; Tang et al. 2017; Ma et al. 2018), such as those next to major roads. The conversion of primary NO exhaust emissions to NO<sub>2</sub>, following the titration of O<sub>3</sub>, also produces a sharply increasing NO<sub>2</sub>/NO<sub>x</sub> ratio with distance from road centre (Fig. 5). In the following sections, a comprehensive evaluation of model performance is presented.

### 3.2 Model evaluation and assessment of emission inventories

Table 4 summarises the performance of ADMS-Urban in Beijing during the APHH-China winter measurement campaign, with comparisons between MEIC Std and MEIC Opt simulations enabling an assessment of the MEIC v1.3 optimisation.

Modelled NO<sub>x</sub> concentrations at the IAP field site display the most substantial differences between the two simulations (Table 4; Fig. 6). Modelled NO<sub>x</sub> concentrations using the MEIC Opt inventory are 149.8 μg m<sup>-3</sup>, 56% lower than the MEIC Std case, leading to NMSE and Fb decreases from 2.35 to 0.63 and 0.93 to 0.17, respectively (Table 4). This enhanced model agreement is reflected in Fig. 6, in which a large proportion of modelled NO<sub>x</sub> values reaching 400-600 μg m<sup>-3</sup> with MEIC Std, up to a factor of six higher than measurements, are reduced to within a factor of two of measured concentrations using MEIC Opt. This result reflects the 63% NO<sub>x</sub> emissions reduction across urban Beijing, over all source sectors, in the optimised inventory (Table 2). However, correlation coefficient (R) values for simulated NO<sub>x</sub> remain low using both emissions inventories, slightly increasing from 0.35 to 0.41 with MEIC Opt. This smaller improvement in the correlation between measured and modelled NO<sub>x</sub> using MEIC Opt, compared to NMSE and Fb, reflects the dependency of R on modelled NO<sub>x</sub> levels that capture the correct temporal variation as well as the overall magnitude of NO<sub>x</sub> measurements. The noise apparent in the measured and simulated NO<sub>x</sub> comparison in Fig. 6 is therefore likely related to either the diurnal emissions profile or meteorological variations.

NO<sub>2</sub> concentrations differ less, with NMSE values of 0.27 and 0.30 for the MEIC Std and MEIC Opt simulations, respectively. However, a greater difference is evident at urban receptor locations, with modelled NO<sub>2</sub> concentrations from the MEIC Opt simulation 12% lower than those with MEIC Std. Across suburban sites, the opposite pattern is seen, with changes in Fb values between measurements and MEIC Std and MEIC Opt simulations ranging from negative (-0.08) to positive (0.02), respectively. Both urban and suburban NO<sub>2</sub> concentration changes, between simulations, reflect the overall redistribution of NO<sub>2</sub> emissions in the MEIC Opt inventory, away from central Beijing and towards the city outskirts (Table 2).

The much greater urban NO<sub>x</sub> concentration difference between the two simulations, as compared to NO<sub>2</sub>, can be attributed to two factors. Firstly, NO<sub>2</sub> concentrations respond in a more non-linear way to NO<sub>x</sub> emission changes than NO<sub>x</sub> concentrations. This has been shown in previous studies (e.g Kurtenbach et al. 2012) and can be explained by the timescales and kinetics involved in the formation and destruction of secondary NO<sub>2</sub>. As NO<sub>x</sub> levels decrease, the production of secondary NO<sub>2</sub> via R4 occurs faster as O<sub>3</sub> concentrations are higher, leading to a slower rate of decrease of NO<sub>2</sub> concentrations compared to NO<sub>x</sub> emissions. Additionally, the proportion of NO<sub>x</sub> directly emitted as NO<sub>2</sub> is greater with MEIC Opt (NO<sub>2</sub>/NO<sub>x</sub> = 0.093) than MEIC Std (NO<sub>2</sub>/NO<sub>x</sub> = 0.068) (Table 2). This is reflected by the much greater reduction, from MEIC Std to MEIC Opt, in domain-aggregated NO<sub>x</sub> emissions (43%), as compared NO<sub>2</sub> (22%) (Table 2).

At urban sites, O<sub>3</sub> concentrations simulated with MEIC Opt are 12.8 μg m<sup>-3</sup>, which is a factor of two greater than those simulated using MEIC Std (6.1 μg m<sup>-3</sup>). Overall, the modelled O<sub>3</sub> concentrations at urban sites using MEIC Opt are in closer agreement with the measurements, reflected by lower Fb and NMSE values of -0.29 and 0.93, respectively, as compared

to -0.95 and 3.2 in the MEIC Std simulations (Table 4). This is caused by both lower urban NO<sub>x</sub> emissions in MEIC Opt and the reduced proportion of remaining NO<sub>x</sub> emitted directly as NO, in MEIC Opt, leading to less O<sub>3</sub> destruction through R4.

445 Contrastingly, higher MEIC Opt NO<sub>x</sub> emissions in suburban Beijing reduce modelled O<sub>3</sub> concentrations by 7%. As a result, modelled O<sub>3</sub> performance across all monitoring stations is substantially improved in the MEIC Opt simulation, with a NMSE reduction from 1.54 to 0.74 and an R value increase from 0.71 to 0.79 (Table 4). These results highlight the strong dependency of O<sub>3</sub> concentration predictions in urban areas, which inform human exposure analyses and influence future emission control implementation, on the accurate spatial variation and magnitude of NO<sub>x</sub> emissions in high resolution emissions inventories.

450 The increase in modelled urban O<sub>3</sub> concentrations following NO<sub>x</sub> emissions reductions also highlights both the negative impact that controls on one pollutant species can have on another as well as the possible need for air quality guidelines that consider multiple pollutants in contrast with the single pollutant-based air quality index used in China (Han et al. 2018).

Figures 7a and 7b illustrate site-specific differences between measured and simulated NO<sub>2</sub> and O<sub>3</sub> concentrations, respectively, using both emissions inventories. It is clear that, despite generally closer model agreement with measurements using MEIC Opt, NO<sub>2</sub> concentrations remain substantially overestimated at urban sites 1 (~14 μg m<sup>-3</sup>) and 2 (~9 μg m<sup>-3</sup>). To help understand the cause of this, the sensitivity of modelled concentrations within 100 m of a road source near site 1 is illustrated in Fig. 8. Concentrations along a cross-road slice, extending 100 m either side of the road, are simulated after halving and doubling the magnitude of emissions of all species from this secondary road. Emissions from all other sources in the model configuration remain the same. Along the road centre, the range of simulated concentrations between emission scenarios is

460 ~10 μg m<sup>-3</sup>, however this difference decreases to ~2 μg m<sup>-3</sup> at a distance of 100 m, which is much lower than modelled NO<sub>2</sub> overestimations produced by MEIC Opt at sites 1 and 2, each located ~80-90 m from the nearest road. Therefore, the high modelled NO<sub>2</sub> at sites 1 and 2 may only be partially attributed to an over-allocation of explicit road source emissions caused by either (a) underlying gridded emissions that are still too high, or (b) not considering traffic volume/speed variations across the domain in road class emission weighting factor estimates. It should also be noted that the physical barriers to pollution dispersion represented by the urban canopy, and specifically street canyons, are not explicitly modelled in this study. This may lead to road emissions dispersing further from the road centre than in reality, therefore contributing to elevated modelled concentrations at greater distances from explicit roads sources (Dédélé and Miskinyte, 2015). The sensitivity of the simulated NO<sub>2</sub>/NO<sub>x</sub> concentration ratio to emission magnitude changes is also shown in Fig. 8. For each emissions scenario, the NO<sub>2</sub>/NO<sub>x</sub> emission ratio remains the same (0.093) (Table 2), however the concentration ratio varies. With doubled NO<sub>x</sub> emissions, the

470 NO<sub>2</sub>/NO<sub>x</sub> ratio is ~0.3 along the road centre, compared to ~0.4 with halved NO<sub>x</sub> emissions (Fig. 8). This difference, which decays to zero at a distance of ~75 m, is mostly driven by PBL dynamics and the mixing of freshly emitted NO<sub>x</sub> into air with a lower NO<sub>2</sub>/NO<sub>x</sub> concentration ratio driven by the impact of higher NO<sub>x</sub> emissions on secondary NO<sub>2</sub> production via R4, as discussed above.

A clear distinction exists between measured PM<sub>2.5</sub> concentrations recorded at the suburban (78 μg m<sup>-3</sup>) and urban (101 μg m<sup>-3</sup>) monitoring stations (Table 4). These values are well in excess of China's annual PM<sub>2.5</sub> National Ambient Air Quality Standard (NAAQS) of 35 μg m<sup>-3</sup>, however concentrations are expected to be higher in winter due to more stable meteorology (Zheng et al. 2015; Li et al. 2017) and enhanced coal combustion for residential heating and cooking and at power plants in neighbouring cities (Chen et al. 2017). Simulated PM<sub>2.5</sub> concentrations, however, do not reflect such an urban-suburban discrepancy, with mean urban values exceeding those at suburban sites by only 9 μg m<sup>-3</sup> and 7 μg m<sup>-3</sup> using MEIC Std and MEIC Opt, respectively (Table 4). Across all monitoring stations, the range in campaign period mean measured concentrations is substantially higher (~40 μg m<sup>-3</sup>) than the simulated range using both MEIC Std (~20 μg m<sup>-3</sup>) and MEIC Opt (~15 μg m<sup>-3</sup>), respectively. These results suggest that either PM<sub>2.5</sub> emission sources are too uniform in magnitude and spatial distribution across the domain in the current model set-up, or that the assumption of a homogeneous background PM<sub>2.5</sub> concentration is invalid. It is likely that, by diluting PM<sub>2.5</sub> emissions within individual grid cells and not explicitly representing point source emissions (e.g. large industrial units), the model is unable to capture the PM<sub>2.5</sub> concentration hotspots that would

485

increase the urban PM<sub>2.5</sub> level increment and improve model agreement with the observed spatial variation. With the exception of simulated PM<sub>2.5</sub> adjacent to major roads, this modelled uniformity in urban PM<sub>2.5</sub> is clearly evident in Fig. 4, in which PM<sub>2.5</sub> concentrations vary by only ~5-10 µg m<sup>-3</sup> across the area enclosed by the Fifth Ring Road. The mean estimated PM<sub>2.5</sub> background concentration is 79 µg m<sup>-3</sup> (Fig. 7), which is higher than both the mean measured concentrations at suburban sites 3 and 10, located to the north. This implies that either the background PM<sub>2.5</sub> level is, in reality, inhomogeneous with lower concentrations to the north and higher to the south of urban Beijing, or that the upwind background monitoring site to the south is too heavily influenced by local emission sources and is not representative of background conditions. The relative contributions from PM<sub>2.5</sub> emission sources and background inhomogeneity to the underestimated spatial variation in PM<sub>2.5</sub> is further discussed in Sect. 3.4.

### 495 3.3 Winter campaign diurnal cycles of NO<sub>2</sub>, O<sub>3</sub> and NO<sub>x</sub>

The diurnal variation of pollutant species in urban areas provides insight into how concentrations are impacted by both diurnal variations in meteorology and temporally varying emissions. The locations of urban stations 1, 12 and IAP, and suburban site 11 are illustrated in Fig. 9, with measured mean diurnal NO<sub>2</sub> concentrations averaged over the campaign period at all four sites compared with those simulated using both the MEIC Std and MEIC Opt inventories in Fig. 10. There are several common differences between modelled and measured concentration profiles at all three urban stations (Fig. 10a, 10c and 10d). Firstly, both simulated NO<sub>2</sub> diurnal cycles at sites 1, 12 and IAP are considerably lower than measurements from 11 pm to 6 am. This discrepancy peaks at 2 am, with simulated concentrations ~20 µg m<sup>-3</sup> and ~30 µg m<sup>-3</sup> lower than measurements, using MEIC Std and MEIC Opt, respectively. Observed NO<sub>2</sub> concentrations at urban sites remain elevated between 11 pm and 6 am, relative to the rest of the day, resulting in a diurnal profile absent of the distinct morning and evening peaks commonly observed in other megacities, such as London (Hood et al. 2018). High nocturnal NO<sub>2</sub> concentration measurements during the APHH-China winter campaign at the IAP field site are also noted by Shi et al. (2019).

Previous studies have attributed the evening influx of heavy duty diesel trucks (HDDTs), banned from commuting within the Fourth Ring Road from 6 am to 11 pm (Zhang et al. 2019), to evening NO<sub>x</sub> concentration increases across urban Beijing of up to 10 µg m<sup>-3</sup> (Wu et al. 2016; Yang et al. 2019). A large proportion of this HDDT fleet originates in other provinces where emission standards are not as strict as those in Beijing (Wang et al. 2011). It is possible, therefore, that in a proxy-based emissions inventory (e.g MEIC), such traffic restrictions and inter-provincial vehicle mobility are not fully accounted for (Zheng et al. 2014). This is supported by the much closer agreement between evening modelled and measured NO<sub>2</sub> at suburban site 11 (Fig. 10b), situated outside the Sixth Ring Road (Fig. 9) and away from the influence of additional nighttime HDDT NO<sub>x</sub> emissions. Additionally, ADMS-Urban makes an approximation when modelling dispersion in calm conditions by applying a minimum wind speed of 0.75 m s<sup>-1</sup> (CERC, 2017). These stable, low wind speed conditions, however, are common in winter in Beijing and have been strongly linked to the acceleration of pollution accumulation during severe winter haze events (Zhang et al. 2015; Zhang et al. 2016; Zhang et al. 2018). Therefore, it is likely that the large early morning NO<sub>2</sub> concentration model underestimations across all three urban sites are a consequence of NO<sub>x</sub> emissions that are too low in magnitude, from 11 pm to 6 am, dispersing into a simulated PBL that may be insufficiently stable due to the use of a minimum wind speed in the model.

From 6-9 am, modelled NO<sub>2</sub> concentrations in both the MEIC Std and MEIC Opt simulations increase sharply (Fig. 10). This is most prominent at site 1, where simulated levels approximately double during this three hour period. This increase corresponds to the release of rush hour traffic-related NO<sub>x</sub> emissions into a stable and shallow morning PBL. Contrastingly, measurements at these sites decline over this early morning period following an evening concentration peak as described above. This overestimation of NO<sub>2</sub> continues throughout the afternoon, with similar profiles at sites 12 and IAP reflecting the close proximity of both receptor locations (~3 km apart) (Fig. 9).

The concurrence of evening rush hour traffic emissions and a stabilising PBL, associated with the reduction in surface heating following sunset, creates a second simulated NO<sub>2</sub> concentration peak at ~6 pm. In contrast to the simulated morning concentration rise, the close agreement between the measured and modelled time of onset and magnitude of this early evening increment indicates that the simulated stability adjustment (Sect. 2.1.2), implemented between 4-7 pm, has successfully accounted for the re-release of stored heat, characteristic of large urban areas.

There is little difference between the diurnal NO<sub>2</sub> concentration profiles simulated using the MEIC Std and MEIC Opt inventories and this is consistent with the model evaluation results described in Sect. 3.2. Simulated NO<sub>2</sub> concentrations across the urban sites are marginally lower using MEIC Opt compared to MEIC Std, with the reverse true at suburban site 11, again reflecting the relocation of emissions out of the urban centre.

The much closer agreement between measured NO<sub>x</sub> concentrations at the IAP field site and those simulated with MEIC Opt compared to MEIC Std, outlined in Sect. 3.2, is further emphasised by the diurnal cycles in Fig. 11. MEIC Opt produces much lower NO<sub>x</sub> concentrations than MEIC Std across all hours of the day (up to a factor of three), peaking during morning and evening rush hour with concentrations of ~200 µg m<sup>-3</sup> and ~250 µg m<sup>-3</sup>, respectively. The simulated NO<sub>2</sub>/NO<sub>x</sub> concentration ratio at IAP produced with MEIC Opt ranges from 0.4 to 0.7 throughout the day, 0.2-0.3 greater than the MEIC Std simulation. This again reflects the combined influences of both the greater NO<sub>2</sub>/NO<sub>x</sub> emission ratio in MEIC Opt (Table 2) and the non-linear response of secondary NO<sub>2</sub> concentrations to NO<sub>x</sub> emission changes, as discussed in Sect. 3.2. Overestimated NO<sub>x</sub> concentrations and underestimated NO<sub>2</sub>/NO<sub>x</sub> concentrations ratios at IAP produced with MEIC Opt indicate that, despite emissions modifications, the magnitude of NO<sub>x</sub> emissions (specifically NO), are too high in the MEIC Opt inventory.

The impact of NO<sub>x</sub> emissions differences on diurnal O<sub>3</sub> concentrations is illustrated in Fig. 12. Using MEIC Std, simulated O<sub>3</sub> concentrations across all three urban sites, are considerably lower than measured values from 8 am to 5 pm, with the measured-modelled difference reaching ~20 µg m<sup>-3</sup> at midday. This reflects the prominence of R4, caused by high urban NO emissions in MEIC Std. The reverse response is seen at site 11, where midday O<sub>3</sub> is overestimated by ~10 µg m<sup>-3</sup> as a result of low MEIC Std NO emissions in suburban versus urban regions. During daylight hours, there is much closer agreement between measured and modelled O<sub>3</sub> across all four sites with MEIC Opt. This reflects the adjusted balance between photochemical production of O<sub>3</sub>, via R3, and its removal via R4, caused by decreased NO<sub>x</sub> emissions in urban areas and increased emissions in suburban areas, in the MEIC Opt inventory. NO<sub>x</sub>-O<sub>3</sub> chemistry is also greatly influenced by proximity to road sources. As shown in Fig. 8 and discussed in Sect. 3.2, roads with higher NO<sub>x</sub> emissions lead to lower NO<sub>2</sub>/NO<sub>x</sub> concentration ratios within distances of 100m and therefore greater O<sub>3</sub> loss through its titration by NO in R4.

#### 3.4 Local and regional contributions to PM<sub>2.5</sub> concentrations

Figure 13 presents the diurnal variation of the range of site-specific campaign period mean measured and simulated PM<sub>2.5</sub> concentrations, using MEIC Opt, across all 12 monitoring network sites. The interquartile range of all network measurements, illustrating the extent to which PM<sub>2.5</sub> concentrations vary spatially across the domain, greatly exceeds that of modelled concentrations for most of the day. This observed range is largest at night and consistently in excess of 20 µg m<sup>-3</sup>, compared to the simulated range of 5-10 µg m<sup>-3</sup>. The measured ranges are additionally sub-divided into those recorded at urban and suburban monitoring sites, with the diurnal median urban PM<sub>2.5</sub> values as much as ~35 µg m<sup>-3</sup> higher than those for suburban sites between 11 pm and 2 am. It is possible that, similarly to the elevated evening NO<sub>2</sub> concentration measurements discussed in Sect. 3.3, this high measured nighttime urban PM<sub>2.5</sub> concentration increment is also related to the influx of HDDTs to central Beijing following the lifting of traffic restrictions from 11 pm to 6 am, with recent studies (Zhang et al. 2015; Wu et al. 2016) reporting a rising contribution from HDDT exhaust emissions to PM<sub>2.5</sub> levels across China. A subsequent reduction of the measured urban-suburban PM<sub>2.5</sub> level discrepancy during daytime hours, reaching ~10 µg m<sup>-3</sup> at midday, coincides with much closer overall agreement between modelled and measured concentrations.

The large difference between mean measured urban and suburban PM<sub>2.5</sub> concentrations throughout the day in Fig. 13 is not captured by the model. This is likely the result of either a lack of heterogeneity in the modelled PM<sub>2.5</sub> emission sources, particularly across urban areas, or that, in reality, substantial non-uniformity in the background concentration exists across the domain. The former is consistent with a number of previous studies on PM<sub>2.5</sub> source apportionment in Beijing, which have suggested that, during extended periods of elevated particulate mass concentrations in winter, local emissions can account for 80% of PM<sub>2.5</sub> concentrations (Li et al. 2017; Wang et al. 2017; Chang et al. 2019). Therefore, as discussed in Sect. 3.2, in order to simulate the high spatial variation of PM<sub>2.5</sub> concentrations, characterised by large urban PM<sub>2.5</sub> concentration increments, higher resolution modelling of primary PM<sub>2.5</sub> emissions, through the inclusion of explicitly represented large point sources is likely to be necessary.

It is also possible that greater secondary aerosol production needs to be included in the model's chemistry scheme, further increasing the simulated urban PM<sub>2.5</sub> increment. Currently in ADMS-Urban, with the exception of ammonium sulphate production, secondary PM<sub>2.5</sub> concentrations are assumed to be included in the upwind background concentration. As the dominant contribution to secondary PM<sub>2.5</sub> in Beijing is reported to be from neighbouring industrial regions to the south (Ma et al. 2017), this assumption seems largely valid. However, the relative local contributions of other secondary components in Beijing, such as ammonium nitrates, are found to be increasing (Wang et al. 2017; Xu et al. 2019; Yang et al. 2019). This is a consequence of the effectiveness of recent SO<sub>2</sub> emission controls and the lack of agricultural ammonia (NH<sub>3</sub>) emissions reductions (Zheng et al. 2018), which have promoted the formation of ammonium nitrate (Xu et al. 2019). Xu et al. (2019) also found the nitrate aerosol to be of increasing importance at night during winter, as a result of its greater stability at lower temperatures, which, coupled with high nighttime NO<sub>2</sub> concentrations (Fig. 10), may further account for the elevated evening PM<sub>2.5</sub> levels (Fig. 13). The applicability of this previous work is possibly limited by the smaller domain size and short timescales of pollution dispersion in this study compared with those necessary for secondary aerosol production. However, future work testing the impact of both the higher resolution representation of PM<sub>2.5</sub> emission sources and additional secondary particle formation pathways within the chemistry scheme is needed to fully understand the potential impact of both on improving agreement between simulated and measured PM<sub>2.5</sub> concentrations (Fig. 13).

The regional contribution to total PM<sub>2.5</sub> concentrations in Beijing has been shown by previous studies to vary from <10% to >90% depending on the time of year and meteorological conditions (He et al. 2015; Liu et al. 2015; Li et al. 2017; Wang et al. 2017). Therefore, the sensitivity of the calculated PM<sub>2.5</sub> background concentration to the methodology used to select the appropriate monitoring site is important and is illustrated in Fig. 14. As described in Sect. 2.1.4, simulated PM<sub>2.5</sub> concentrations include a wind direction-dependent upwind background contribution calculated using either of two sites to the north or one to the south of urban Beijing. Figure 14 shows the diurnal range of calculated upwind background values during the winter campaign, with the corresponding range of background PM<sub>2.5</sub> calculated by instead selecting the minimum hourly concentration across the monitoring network, matching the methodology used to determine background concentrations for gaseous species.

For each hour, the upwind background PM<sub>2.5</sub> upper quartile, median and lower quartile greatly exceed the corresponding values when using the minimum background methodology. This discrepancy is greatest for the upper quartile values and peaks during morning and evening rush hour, reaching ~80 µg m<sup>-3</sup> at 5 pm (Fig. 14). The lower whiskers, however, denoting the lowest datum lying within 1.5 times the interquartile range of the lower quartile, are common across both sets of PM<sub>2.5</sub> background diurnal cycles. Interpretation of these results is assisted by Fig. 15, which presents hourly wind vectors and PM<sub>2.5</sub> time series measurements throughout the campaign at all three upwind sites as well as urban sites 1 and 2. It is clear that the highest upwind PM<sub>2.5</sub> background concentrations occur when values at the additional site to the southeast of urban Beijing (site 14) are selected during periods of southerly winds (Fig. 15). The lowest background concentrations, therefore, can be attributed to either of the northerly sites (site 3 and site 10). Northerly winds advect clean air originating over the relatively unpolluted mountainous regions into urban Beijing (Tie et al. 2015). This switch in wind directions creates a saw-tooth pattern,

with pollution episodes initially consisting of a slow build-up phase, associated with stagnant southerly winds, and culminating with sharp concentration drops related to the influx of cold northerly air (Li et al. 2017; Wang et al. 2017). A clear example of this, from 23-27 November, is shown in Fig. 15.

615 PM<sub>2.5</sub> concentrations at site 14, situated in the south-eastern corner of the model domain are consistently higher than those measured at sites located in central Beijing. This monitoring station is located in the built-up Guangyang District of Langfang in Hebei province and is not in the immediate vicinity of any large point sources. Therefore, this region is possibly more heavily influenced by regional PM<sub>2.5</sub> advected from industrial towns and cities to the south. This highlights an important limitation of our study, which assumes a homogeneous background concentration for each species; this assumption may not  
620 be valid across such a large and complex urban area.

Both local PM<sub>2.5</sub> emission sources not represented in our study and background inhomogeneity appear to contribute substantially to differences in the spatial and temporal variation of measured and modelled PM<sub>2.5</sub> concentrations. However, the large diurnal variability in measured PM<sub>2.5</sub> concentration ranges across the domain (Fig. 13), not captured by the model, is more likely the influence of local emission sources, with longer timescales required for background PM<sub>2.5</sub> concentration  
625 variability driven by regional transport.

### 3.5 Impact of explicit road source modelling

In this section, we investigate the sensitivity of the simulated NO<sub>2</sub> concentrations to the inclusion of explicit road source emissions. Simulations that use aggregate 3-D grid sources alone are much less computationally expensive than those that also incorporate explicit road source emissions and allow studies to be performed with ADMS-Urban in urban areas where detailed  
630 road network information is unavailable. In Fig. 16, measured NO<sub>2</sub> concentrations averaged across the campaign are compared with those simulated using 3-D grid and explicit road sources, as well as 3-D grid sources only, derived from the MEIC Opt emissions inventory. By resolving road traffic emissions into explicitly represented road sources, as opposed to using gridded emissions only, mean modelled NO<sub>2</sub> concentrations across urban stations increase from 62.8 µg m<sup>-3</sup> to 71.4 µg m<sup>-3</sup> (Table 5). This modelled urban NO<sub>2</sub> concentration increase results in a Fb value improvement from -0.13 to 0 (Table 5) reflecting the greater NO<sub>2</sub> levels simulated by the model at locations in close proximity to explicit roads. By using grid sources only, the road traffic emissions are diluted over each 3 x 3 km grid cell and the strong concentration gradients associated with a region densely populated by major roads, illustrated in Fig. 4, are not captured. Similarly, Dédelé and Miskinyté (2015) and Hood et al. (2018) found that increased traffic emissions due related to higher traffic volume and adjusted emission factors, respectively, produced improved Fb values using ADMS-Urban. The corresponding Fb value improvement, at urban sites, from -0.13 to 0  
635 (Table 5), reflects the negative impact that diluting road traffic emissions over each 3 x 3 km grid cell has on simulated and observed NO<sub>2</sub> level agreement across a region densely populated by major roads.

More accurate model predictions next to roads can lead to better assessments of human exposure levels to pollutant species and is evidence of the successful implementation of the top-down approach to estimating explicit road traffic emissions used in this study. However, it is also clear from Fig. 16 that agreement between modelled and measured NO<sub>2</sub> concentrations at  
645 sites 1 and 2 is substantially poorer when using explicit road sources than with the grid source only simulation. The model evaluation statistics for all monitoring sites (Table 5), reflect this with increases in NMSE from 0.28 to 0.3 and decreases in R from 0.59 to 0.53 when modelling road emissions explicitly. As discussed in Sect. 3.2, this highlights the impact that the assumption of constant traffic activity, high underlying gridded emissions or the absence of street canyon and urban canopy modelling can have on simulated concentrations at certain near-road locations.

650 Minimal R value changes and a much lower Fb improvement, -0.03 to 0.02, are seen across suburban compared to urban areas, following the inclusion of explicit road source emissions. This reflects the lower density of roads in suburban areas (Fig. 4) and therefore the absence of strong concentration gradients that enhance NO<sub>2</sub> levels at near-road urban locations. The relative influence of diffuse emissions contained within the underlying gridded emission sources on simulated pollutant

Formatted: Space After: 0 pt

655 concentrations is therefore more prominent with distance from Beijing's urban centre, with previous studies specifically highlighting the persisting importance of residential coal combustion for heating and cooking during winter in suburban and rural Beijing (Cai et al. 2018; Li et al. 2018). Little change is seen across suburban areas with the inclusion of explicit road source emissions, reflecting the lower density of roads and more dominant contribution from diffuse emissions with distance away from Beijing's urban centre.

### 3.6 Accounting for additional evening NO<sub>x</sub> emission source

660 In this section, the influence of modifying the MEIC diurnal emissions profile, used for all previous simulations, to account for additional sources of nighttime NO<sub>x</sub> emissions is examined. As discussed in Sect. 3.3, a likely explanation for the simulated underestimate in nocturnal NO<sub>x</sub> and NO<sub>2</sub> concentrations is that an additional evening NO<sub>x</sub> emission source is not accounted for in the emissions inventories. The timing of these peak NO<sub>2</sub> and NO<sub>x</sub> measurements, between 11 pm and 6 am, coincides with the influx of HDDTs within Beijing's Fourth Ring Road.

665 Figure 17 presents the standard MEIC diurnal emissions profile (DP\_MEIC), and two alternative profiles, DP\_25 and DP\_50, constructed by increasing the standard MEIC profile factors between 11 pm and 6 am by ~0.25 and ~0.5, respectively, to account for additional nighttime HDDT emissions. For both modified emissions profiles, in order to retain the same 24-hour emissions total, DP\_MEIC is further adjusted between 7 am to 10 pm, by magnitudes that also preserve the timings of the morning and evening emissions peaks associated with rush hour traffic. The weekend emissions profile, characterised by a delayed morning peak and ~30% reduced total daily traffic emissions, is kept unchanged for all three sensitivity simulations. Campaign period mean diurnal profiles of NO<sub>2</sub> concentrations, simulated using the diurnal emissions profiles shown in Fig. 17, are presented in Fig. 18. At suburban site 11, the close agreement between simulated and measured NO<sub>2</sub> concentrations using DP\_MEIC is strengthened further by increasing the proportion of emissions released at night relative to the daytime. Modelled NO<sub>2</sub> level overestimations throughout the morning and afternoon hours at sites 12 and IAP using DP\_MEIC are reduced when applying the two modified emissions profiles. However, at site 1 the application of DP\_50 is unable to reduce daytime NO<sub>2</sub> concentrations substantially, which is likely related again to the effect of overestimated emissions along the nearest explicit road source (Fig. 8). The evening NO<sub>2</sub> concentration is underestimated at sites 1, 12 and IAP, using DP\_MEIC, and this is successively reduced by a small amount with DP\_25 and DP\_50. The remaining evening differences suggest that, although the inclusion of higher nighttime emissions improves agreement, other possible issues exist related to ADMS-urban's inability to model dispersion at very low wind speeds; inaccurate underlying gridded emissions; the simplified GRS chemistry scheme; the exclusion of street canyon and urban canopy modelling or PBL dynamics.

### 3.7 The influence of boundary layer height and stability on diurnal NO<sub>2</sub> concentrations

685 In this section, the impact of PBLH and stability on diurnal NO<sub>2</sub> concentrations is explored with further sensitivity simulations. The space into which emitted plumes of pollutants can disperse and mix is determined by the PBLH. Figure 19 shows the difference between measured and modelled PBLHs and their impact on simulated diurnal NO<sub>2</sub> concentrations. Differences between the PBLH simulated without evening stability adjustment and the observed PBLH (Fig. 19) are characterised by a daytime overprediction and nighttime underprediction. At 3 pm, the rapidly growing convective PBL peaks at ~1100 m, exceeding the observed heights by ~200 m. This difference between observed and simulated PBLHs could be a result of an overestimation of the solar radiation-driven surface sensible heat flux and mechanically-driven turbulent flux values, which are the principal parameters impacting the modelled PBLH. Additionally, due to complex cloud physics, detecting the exact limit of vertical mixing is difficult in the presence of low level stratiform clouds, which form frequently in Beijing during winter, and may further account for low PBLHs derived from ceilometer observations (Kotthaus and Grimmond, 2018). After sunset at 5 pm, the modelled PBLH shrinks to ~200 m, 400 m below the measured height. This sharp transition between an

695 unstable and stable modelled PBL is a consequence of ADMS-urban not accounting for the UHI effect in its surface energy  
balance calculations, as described in 2.1.2.

The early evening stability adjustment (Sect. 2.1.2) applied to all previous simulations in this study replicates the  
effect of the UHI by reducing PBL stability between 4-7 pm. By applying the stability modification, early evening modelled  
PBLH increases and reaches ~1300 m by 6 pm before sharply decreasing to ~200 m by 8 pm. Note that directly input PBLH  
measurements are unaffected by changes to  $L_{MO}$  and surface heat flux terms. The stability adjustment reduces  $NO_2$   
700 concentrations simulated at 4 pm using modelled and measured PBLHs by ~40  $\mu g\ m^{-3}$  and ~15  $\mu g\ m^{-3}$ , respectively, greatly  
improving agreement with measurements. The sharp morning modelled  $NO_2$  concentration rise, peaking at 9 am, decreases by  
~10  $\mu g\ m^{-3}$  through use of the measured PBLH alone. However, application of a similar PBL stability adjustment, between 7-  
10 am, would likely reduce the early morning PBLH underestimation and further weaken the modelled  $NO_2$  concentration rise  
associated with the input of rush hour-related  $NO_x$  emissions into a morning PBL that is currently too stable and too shallow  
705 compared to observations.

The results suggest that although atmospheric stability modifications ~~have~~ a strong impact on  $NO_2$  concentrations, the use of  
observed PBLH instead of modelled heights has little effect. This is clearest outside the hours in which the stability  
correction has been applied, when large (~300  $\mu g\ m^{-3}$ ) measured and modelled mid-afternoon and nighttime PBLH  
710 discrepancies have negligible impact on simulated  $NO_2$  concentrations. The greater impact of PBL stability changes alone,  
however, is clearly evidenced by the ~15  $\mu g\ m^{-3}$  difference at 4 pm between simulations using measured PBLHs with and  
without the stability correction. notable at night, when much greater measured nocturnal PBLHs have negligible impact on  
simulated  $NO_2$  levels. This dominant influence of PBL stability is possibly related to the ~~major~~ dominant impact in the  
model configuration of near-surface traffic emissions and the exclusion of elevated point sources, with pollution dispersion  
from the latter more likely to be restricted by low PBLHs which would then further affect modelled  $NO_2$  levels. compared to  
715 elevated sources, with dispersion of the latter more likely to be restricted by low PBLHs.

#### 4 Conclusions

In this study, street-scale resolution concentrations of  $NO_x$ ,  $NO_2$ ,  $O_3$  and  $PM_{2.5}$  are simulated for Beijing, using the Gaussian  
pollution dispersion and chemistry model, ADMS-Urban. Simulations for the APHH-China winter measurement campaign  
period (5 November 2016 – 10 December 2016), are driven by an explicit source road traffic emissions inventory, developed  
720 for this work using a pseudo top-down methodology. This approach, which involves apportioning an underlying high-  
resolution gridded emissions inventory onto Beijing's spatial road network, provided by OpenStreetMap, may be applied to  
investigate the air quality in other cities where detailed bottom-up traffic emissions inventories are unavailable.

Measurements recorded at 12 of Beijing's air quality monitoring network stations and at the Institute of Atmospheric  
Physics (IAP) field site are compared with simulated pollutant levels generated by the Multi-resolution Emission Inventory  
725 for China v1.3 (MEIC Std), at 3 km resolution, and an optimised version of the same inventory (MEIC Opt). MEIC Opt, which  
is based on campaign measurements, has lower emissions across urban Beijing (within the Sixth Ring Road), and higher  
emissions in surrounding suburban areas, resulting in greatly improved agreement between observed and simulated  
concentrations for all species. Most notably, driven by  $NO$  emission changes, simulated mean  $NO_x$  concentrations at the IAP  
site are lower by more than a factor of two using MEIC Opt compared to the MEIC Std inventory. Consequently, modelled  
730 urban  $O_3$  concentrations increase by 109%, with suburban  $O_3$  concentrations decreasing by 7% in simulations performed with  
MEIC Opt.

The inclusion of explicit road sources allows sharp  $NO_2$  concentration gradients adjacent to major roads to be resolved,  
leading to generally closer agreement between network measurements and simulated concentrations. However, limitations of  
the model configuration can lead to modelled  $NO_2$  levels that are substantially higher than measurements at some near-road

735 (~100 m) sites. These model uncertainties stem from the application of uniform weighting factors to roads of the same  
classification (thus neglecting traffic activity variations), the assumptions inherent to the underlying gridded inventory, and  
exclusion of the physical barriers to pollution dispersion created by street canyons. [Future work could focus on refining the  
explicit road emissions network created here by testing the impact of adjusting weighting factors for different pollutants and  
across urban and suburban areas to better account for the impact of traffic congestion and vehicle type, such as HDDTs, on  
emissions along different road classifications.](#)

740 Differences in the diurnal variability of measured and simulated NO<sub>2</sub> concentrations during the winter campaign  
period reveal features related to emissions (e.g. local driving restrictions) and the Urban Heat Island (UHI), that air quality  
modelling studies over large urban areas should consider. For instance, measured NO<sub>2</sub> concentrations at urban monitoring sites  
situated close to roads can reach nighttime values above 80 µg m<sup>-3</sup>, exceeding both morning and evening rush hour levels. This  
745 pattern is not reproduced in the simulated NO<sub>x</sub> concentrations and is consistent with the evening influx of heavy duty diesel  
trucks (HDDTs), banned from traversing within the Fourth Ring Road between 6 am and 11 pm. The increase in HDDT traffic  
at night across urban Beijing is therefore an important local emission source that needs to be included in MEIC and other  
proxy-based emission inventories. Additionally, modifying modelled PBL stability parameters to replicate early evening (4-7  
750 pm) instability driven by the delayed release of heat stored in the urban fabric, improves the diurnal variation in simulated NO<sub>2</sub>  
concentrations. A similar modification may improve morning model predictions, although it would be difficult to use the  
presence of a UHI to justify this.

The range in measured PM<sub>2.5</sub> concentrations across the monitoring network for the campaign period (~40 µg m<sup>-3</sup>) is  
much higher than the corresponding simulated range using both MEIC Std (~20 µg m<sup>-3</sup>) and MEIC Opt (~15 µg m<sup>-3</sup>). The  
large difference between measured suburban and urban PM<sub>2.5</sub> levels is also not captured by the model and may indicate any or  
755 all of the following: (a) PM<sub>2.5</sub> emissions are too low in magnitude and not represented at sufficiently high resolution,  
particularly across urban areas, (b) the simplified GRS chemistry scheme needs to be modified to increase contributions from  
locally produced secondary PM<sub>2.5</sub>, or (c) the assumption of a homogeneous background concentration across complex  
megacities, such as Beijing, which are heavily influenced by the advection of regional pollution, is not valid.  
Sensitivity studies have shown that using explicit road source emissions; including an additional nighttime emission source;  
760 and accounting for UHI effects, through enhanced early evening instability conditions, can produce closer agreement between  
simulated and measured NO<sub>2</sub> concentrations.

Street-level modelling, along with the open data sources and methodologies used here, may be applied for future work  
elsewhere. Quantifying spatio-temporal pollutant distributions at such fine scales is essential for human health exposure-related  
studies, and for informing choices on the emission controls of specific sectors.

765 *Author contributions.* MB set up and ran the model with support from JS. MB processed the model outputs with support from  
JS. This manuscript was written by MB with guidance from JS, RMD, OW and DC. All authors read and improved the  
manuscript. ZS, JL, FAS, SK and SG provided measurement data. JL, QZ, RW and MH provided and processed the emissions  
data.

770 *Acknowledgements.* This work was funded by the UK Natural Environment Research Council (NERC) Industrial studentship  
scheme with CASE support provided by Cambridge Environmental Research Consultants (CERC) under grant code  
NE/N0077941/1. We would also like to acknowledge the APHH-China programme funded by NERC under the grant codes  
NE/N006941/1, NE/N006925/1 and NE/N006976/1.

775 **References**

Afiq, W. M. Y., Azwadi, C. S. N., and Saqr, K. M.: Effects of buildings aspect ratio, wind speed and wind direction on flow structure and pollutant dispersion in symmetric street canyons: A review, *International Journal of Mechanical and Materials Engineering (IJMME)*, 7, 158-165, 2012.

Aktas, Y. D., Stocker, J., Carruthers, D., Hunt, J.: A sensitivity study relating to neighbourhood-scale fast local urban climate modelling within the built environment, *Proced. Engin.*, 198, 589-599, <https://doi.org/10.1016/j.proeng.2017.07.113>, 2017.

Anandakumar, K.: A study on the partition of net radiation into heat fluxes on a dry asphalt surface, *Atmos. Environ.*, 33, 3911-3918, [https://doi.org/10.1016/S1352-2310\(99\)00133-8](https://doi.org/10.1016/S1352-2310(99)00133-8), 1999.

Barlow, J. F., Halios, C. H., lane, S. E., Wood, C. R.: Observations of urban boundary layer structure during a strong urban heat island event, *Environ. Fluid Mech.*, 15, 373-398, <https://doi.org/10.1007/s10652-014-9335-6>, 2015.

785 Bates, J. T., Pennington, A. F., Zhai, X., Friberg, M. D., Metcalf, F., Darrow, L., Strickland, M., Mulholland, J., Russell, A.: Application and evaluation of two model fusion approaches to obtain ambient air pollutant concentrations at a fine spatial resolution (250m) in Atlanta, *Environment Modelling and Software*, 109, 182-190, <https://doi.org/10.1016/j.envsoft.2018.06.008>, 2018.

Cai, H., and Xie, S.: Traffic-related air pollution modelling during the 2008 Beijing Olympic Games: The effects of an odd-even day traffic restriction scheme, *Science of The Total Environment*, 408, 1935-1948, <https://doi.org/10.1016/j.scitotenv.2011.01.025>, 2011.

790 <https://doi.org/10.1016/j.scitotenv.2011.01.025>, 2011.

[Cai, S., Li, Q., Wang, S., Chen, J., Ding, D., Zhao, B., Yang, D., Hao, J.: Pollutant emissions from residential combustion and reduction strategies estimated via a village-based emission inventory in Beijing, \*Environ. Poll.\*, 238, 230-237, <https://doi.org/10.1016/j.envpol.2018.03.036>, 2018.](https://doi.org/10.1016/j.scitotenv.2011.01.025)

795 Cambridge Environmental Research Consultants (CERC): ADMS-Urban Urban Air Quality Management System Version 4.1 User Guide, available at: [http://www.cerc.co.uk/environmental-software/assets/data/doc\\_userguides/CERC\\_ADMS-Urban4.1.1\\_User\\_Guide.pdf](http://www.cerc.co.uk/environmental-software/assets/data/doc_userguides/CERC_ADMS-Urban4.1.1_User_Guide.pdf), (last access: 6 June 2019), 2017.

Carruthers, D. J.: airTEXT air quality forecasting system, Towards eEnvironment, GMES meeting, Prague, Czech Republic, 2009.

800 Chang, X., Wang, S., Zhao, B., Xing, J., Liu, X., Wei, L., Song, Y., Wu, W., Cai, S., Zheng, H., Ding, D., Zheng, M.: Contributions of inter-city and regional transport to PM<sub>2.5</sub> concentrations in the Beijing-Tianjin-Hebei region and its implications on regional joint air pollution, *Science of The Total Environment*, 660, 1191-1200, <https://doi.org/10.1016/j.scitotenv.2018.12.474>, 2019.

Chen, C-H., Kan, H-D., Huang, C., Li, L., Zhang, Y-H., Chen, R-J., Chen, B-H.: Impact of ambient air pollution on public health under various traffic policies in Shanghai, China, *Biomedical and Environmental Sciences*, 22, 210-215, [https://doi.org/10.1016/S0895-3988\(09\)60047-7](https://doi.org/10.1016/S0895-3988(09)60047-7), 2009.

805 Chen, W., Yan, L., Zhao, H.: Seasonal variations of atmospheric pollution and air quality in Beijing, *Atmosphere*, 6, 1753-1770, <https://doi.org/10.3390/atmos6111753>, 2015.

Chen, S., Xu, L., Zhang, Y., Chen, B., Wang, X., Zhang, X., Zheng, M., Chen, J., Wang, W., Sun, Y., Fu, P., Wang, Z., Li, W.: Direct observations of organic aerosols in common wintertime hazes in North China: insights into direct emissions from Chinese residential stoves, *Atmos. Chem. Phys.*, 17, 1259-1270, <https://doi.org/10.5194/acp-17-1259-2017>, 2017.

810 Cheng, J., Su, J., Cui, T., Li, X., Dong, X., Sun, F., Yang, Y., Tong, D., Zheng, Y., Li, J., Zhang, Q., He, K.: Dominant role of emission reduction in PM<sub>2.5</sub> air quality improvement in Beijing during 2013-2017: a model-based decomposition analysis, *Atmos. Chem. Phys. Discuss.*, <https://doi.org/10.5194/acp-19-6125-2019> <https://doi.org/10.5194/acp-2018-1145>, 2019.

815 Cimorelli, A. J., Perry, S. G., Venkatram, A., Weil, J. C., Paine, R. J., Wilson, R. B., Lee, R. F., Peters, W. D., Brode, R. W.: AERMOD: A dispersion model for industrial source applications. Part I: General model formulation and boundary layer characterisation, *J. App. Met.*, 44, 682-693, <https://doi.org/10.1175/JAM2227.1.2005>

Formatted: Font: (Default) Times New Roman, 10 pt

Formatted: Default Paragraph Font

Formatted: Font: (Default) Times New Roman, 10 pt

Formatted: Default Paragraph Font

Cui, J., Lang, J., Chen, T., Mao, S., Cheng, S., Wang, Z., Cheng, N.: A framework for investigating the air quality variation characteristics based on the monitoring data: Case study for Beijing during 2013-2016, *J. Env. Sci.*, 81, 225-237, <https://doi.org/10.1016/j.jes.2019.01.009>, 2019.

820 <https://doi.org/10.1016/j.jes.2019.01.009>, 2019.

Dédélé, A., Miskinyté, A.: The statistical evaluation and comparison of ADMS-Urban model for the prediction of nitrogen dioxide with air quality monitoring network, *Environ. Monit. Assess.*, 187, <https://doi.org/10.1007/s10661-015-4810-1>, 2015.

Fu, L., Hao, J., Hertel, O., and Berkowicz, R.: Modeling traffic-related air pollution in street canyons of Beijing, *Journal of the Air & Waste Management Association*, 50, 2060-2066, <https://doi.org/10.1080/10473289.2000.10464234>, 2000.

825 GBD 2016 Risk Factors Collaborators: Global, regional, and national comparative risk assessment of 84 behavioural, environmental and occupational, and metabolic risks or clusters of risks, 1990–2016: a systematic analysis for the Global Burden of Disease Study 2016, *Lancet*, 390, 1345-422, 2017.

Grimmond, C. S. B., Oke, T. R.: Heat storage in urban areas: local-scale observations and evaluation of a simple model, *J. App. Met.*, 38, 922-940, [https://doi.org/10.1175/1520-0450\(1999\)038<0922:HSIUAL>2.0.CO;2](https://doi.org/10.1175/1520-0450(1999)038<0922:HSIUAL>2.0.CO;2), 1999.

830 Hamilton, I., Stocker, J., Evans, S., Davies, S., Davies, M., Carruthers, D.: The impact of the London Olympic parkland on the urban heat island, *J. Build. Perf. Sim.*, 7, 119-132, <https://doi.org/10.1080/19401493.2013.791343>, 2014.

Han, L., Zhou, W., Pickett, S. T., Li, W., Qian, Y.: Multicontaminant air pollution in Chinese cities, *Bull. World Health Organ.*, 96, 233-242, doi: 10.2471/BLT.17.195560, 2018.

835 Hong, C., Zhang, Q., He, K., Guan, D., Li, M., Liu, F., Zheng, B.: Variations of China's emission estimates: response to uncertainties in energy statistics, *Atmos. Chem. Phys.*, 17, 1227-1239, <https://doi.org/10.5194/acp-17-1227-2017>, 2017.

Hood, C., MacKenzie, I., Stocker, J., Johnson, K., Carruthers, D., Vieno, M., Doherty, R.: Air quality simulations for London using a coupled regional-to-local modelling system, *Atmos. Chem. Phys.*, 18, 11221-11245, <https://doi.org/10.5194/acp-18-11221-2018>, 2018.

840 Jing, B., Wu, L., Mao, H., Gong, S., He, J., Zou, C., Song, G., Li, X., Wu, Z.: Development of a vehicle emission inventory with high temporal-spatial resolution based on NRT traffic data and its impact on air pollution in Beijing – Part 1: Development and evaluation of vehicle emission inventory, *Atmos. Chem. Phys.*, 16, 3161-3170, doi:10.5194/acp-16-3161-2016, 2016.

Karamchandani, P., Zhang, Y., Chen, S-Y., Balmori-Bronson, R.: Development of an extended chemical mechanism for global-through-urban applications, *Atmos. Pol. Res.*, 3, 1-24, <https://doi.org/10.5094/APR.2011.047>, 2012.

845 Kotthaus, S., Grimmond, C. S. B.: Atmospheric boundary-layer characteristics from ceilometer measurements. Part 1: A new method to track mixed layer height and classify clouds, *Quarterly Journal of the Royal Meteorological Society*, 144, 1525-1538, DOI: 10.1002/qj.3299, 2018.

Kurtenbach, R., Kleffmann, J., Niedojadlo, A., Wiesen, P.: primary NO<sub>2</sub> emissions and their impact on air quality in traffic environments in Germany, *Environ. Sci. Eur.*, 24, <https://doi.org/10.1186/2190-4715-24-21>, 2012.

850 Li, J., Du, H., Wang, Z., Sun, Y., Yang, W., Li, J., Tang, X., Fu, P.: Rapid formation of a severe regional winter haze episode over a mega-city cluster on the North China Plain, *Environ. Poll.*, 223, 605-615, <https://doi.org/10.1016/j.envpol.2017.01.063>, 2017.

Li, X., Wu, J., Elser, M., Feng, T., Cao, J., El-Haddad, I., Huang, R., Tie, X., Prévot, A. S. H., Li, G.: Contributions of residential coal combustion to the air quality in Beijing-Tianjin-Hebei (BTH), China: a case study, *Atmos. Chem. Phys.*, 18, 10675-10691, <https://doi.org/10.5194/acp-18-10675-2018>, 2018.

855 Liang, Z., Yang, Y., Qian, Z., Ruan, Z., Chang, J., Vaughn, M. G., Zhao, Q., Lin, H.: Ambient PM<sub>2.5</sub> and birth outcomes: Estimating the association and attributable risk using a birth cohort study in nine Chinese cities, *Environ. Int.*, 126, 329-335, <https://doi.org/10.1016/j.envint.2019.02.017>, 2019.

Liu, W., Ji, C., Zhong, J., Jiang, X., Zheng, Z.: Temporal characteristics of the Beijing urban heat island, *Theor. App. Clim.*, 87, <https://doi.org/10.1007/s00704-005-0192-6>, 2007.

Formatted: Font: (Default) Times New Roman, 10 pt

Formatted: Default Paragraph Font

Formatted: Font: (Default) Times New Roman, 10 pt

Formatted: Font: (Default) Times New Roman, 10 pt

860 Liu, F., Zhang, Q., Tong, D., Zheng, B., Li, M., Huo, H., He, K. B.: High-resolution inventory of technologies, activities, and emissions of coal-fired power plants in China from 1990 to 2010, *Atmos. Chem. Phys.*, 15, 13299-13317, <https://doi.org/10.5194/acp-15-13299-2015>, 2015.

Liu, F., Zhang, Q., Van der A, R. J., Zheng, B., Tong, D., Yan, L., Zheng, Y., He, K.: Recent reduction in NO<sub>x</sub> emissions over China: synthesis of satellite observations and emission inventories, *Environ. Res. Lett.*, 11, doi:10.1088/1748-9326/11/11/114002, 2016.

865 Liu, L., Huang, X., Ding, A., Fu, C.: Dust-induced radiative feedbacks in north China: A dust storm episode modelling study using WRF-Chem, *Atmos. Environ.*, 129, 43-54, <https://doi.org/10.1016/j.atmosenv.2016.01.019>, 2016.

Liu, F., Beirle, S., Zhang, Q., Van der A, R. J., Zheng, B., Tong, D., He, K.: NO<sub>x</sub> emission trends over Chinese cities estimated from OMI observations during 2005 to 2015, *Atmos. Chem. Phys.*, 17, 9261-9275, <https://doi.org/10.5194/acp-17-9261-2017>, 2017.

870 [Lugon, L., Sartelet, K., Kim, Y., Vigneron, J., Chrétien, O.: Street-in-Grid modeling of gas-phase pollutants in Paris city, Atmos. Chem. Phys. Discuss., https://doi.org/10.5194/acp-2019-1087, in review, 2019.](#)

Ma, Q., Wu, Y., Zhang, D., Wang, X., Xia, W., Xia, Y., Liu, X., Tian, P., Han, Z., Xia, X., Wang, Y., Zhang, R.: Roles of regional transport and heterogeneous reactions in the PM<sub>2.5</sub> increase during winter haze episodes in Beijing, *Science of The Total Environment*, 599-600, 246-253, <https://doi.org/10.1016/j.scitotenv.2017.04.193>, 2017.

875 Ma, J., Chu, B., Liu, J., Liu, Y., Zhang, H. He, H.: NO<sub>x</sub> promotion of SO<sub>2</sub> conversion to sulfate: An important mechanism for the occurrence of heavy haze during winter in Beijing, *Environ. Poll.*, 223, 662-669, <https://doi.org/10.1016/j.envpol.2017.10.103>, 2018.

Malkin, T. L., Heard, D. E., Hood, C., Stocker, J., Carruthers, D., MacKenzie, I. A., Doherty, R. M., Vieno, M., Lee, J., Kleffmann, J., Laufs, S., Whalley, L. K.: Assessing chemistry schemes and constraints in air quality models used to predict ozone in London against the detailed Master Chemical Mechanism, *Faraday. Discuss.*, 189, DOI: 10.1039/c5fd00218d, 2016.

McHugh, C. A., Sheng, X., Carruthers, D. J.: Using ADMS models for air quality assessment and management in China, *Chinese Journal of Population Resources and Environment*, 3, 2005.

Mohan, M., Bhati, S., Sreenivas, A., Marrapu, P.: Performance evaluation of AERMOD and ADMS-Urban for total suspended particulate matter concentrations in megacity Delhi, *Aerosol and Air Quality Research*, 11, 883-894, doi: 10.4209/aaqr.2011.05.0065, 2011.

885 [Munir, S., Habeebullah, T. M.: Vehicular emissions on main roads in Makkah, Saudi Arabia — a dispersion modelling study, Arab. J. Geosci., 11, https://doi.org/10.1007/s12517-018-3857-z, 2018.](#) National Bureau of Statistics: *China Statistical Yearbook for Regional Economy 2014*, China Statistics Press, Beijing, China, 2014.

890 [Ni, Z., Luo, K., Gao, Y., Gao, X., Fan, J., Cen, K.: Potential air quality improvements from ultralow emissions at coal-fired power plants in China, Aerosol and Air Quality Research, 18, 1944-1951, doi: 10.4209/aaqr.2018.02.0070, 2018.](#) Oak Ridge National Laboratory (ORNL): *LandScan Global Population Database*, Oak Ridge National Laboratory, Oak Ridge, TN, USA, 2013.

Oke, T. R.: The energetic basis of the urban heat island, *Quart. J. R. Met. Soc.*, 108, 1-24, 1982.

895 OpenStreetMap, available at: <http://openstreetmap.org>, (last access: 6 June 2019), 2019.

Owen, B., Edmunds, H. A., Carruthers, D. J., Singles, R. J.: Prediction of total oxides of nitrogen and nitrogen dioxide concentrations in a large urban area using a new generation urban scale dispersion model with integral chemistry model, *Atmos. Environ.*, 34, 397-406, [https://doi.org/10.1016/S1352-2310\(99\)00332-5](https://doi.org/10.1016/S1352-2310(99)00332-5), 2000.

900 Patryl, L., Galeriu, D.: Statistical performances measures – models comparison, *French Alternative Energies and Atomic Energy Commission*, 2011.

Formatted: Font: (Default) Times New Roman, 10 pt

Formatted: Font: (Default) Times New Roman, 10 pt

Formatted: Font: (Default) Times New Roman, 10 pt

Formatted: English (United Kingdom)

Formatted: German (Germany)

Formatted: Default Paragraph Font, English (United Kingdom)

Formatted: German (Germany)

Formatted: Font: (Default) Times New Roman, 10 pt

Petaja, T., Jarvi, L., Kerminen, V.-M., Ding, A. J., Sun, J. N., Nie, W., Kujansuu, J., Virkkula, A., Yang, X., Fu, C. B., Zilitinkevich, S., Kulmala, M.: Enhanced air pollution via aerosol-boundary layer feedback in China, *Scientific Reports*, 6, DOI: 10.1038/srep18998, 2016.

905 Qi, J., Zheng, B., Li, M., Yu, F., Chen, C., Liu, F., Zhou, X., Yuan, J., Zhang, Q., He, K.: A high-resolution air pollutants emission inventory in 2013 for the Beijing-Tianjin-Hebei region, China, *Atmos. Environ.*, 170, 156-168, <https://doi.org/10.1016/j.atmosenv.2017.09.039>, 2017.

Sarwar, G., Luecken, D.: Impact of an updated carbon bond mechanism on predictions from the CMAQ modelling system: Preliminary assessment, *J. App. Met. Clim.*, 47, <https://doi.org/10.1175/2007JAMC1393.1>, 2008.

910 Shi, Z., Vu, T., Kotthaus, S., Grimmond, S., Harrison, R. M., Yue, S., Zhu, T., Lee, J., Han, Y., Demuzere, M., Dunmore, R. E., Ren, L., Liu, D., Wang, Y., Wild, O., Allan, J., Barlow, J., Beddows, D., Bloss, W. J., Carruthers, D., Carslaw, D. C., Chatzidiakou, L., Crilley, L., Coe, H., Dai, T., Doherty, R., Duan, F., Fu, P., Ge, B., Ge, M., Guan, D., Hamilton, J. F., He, K., Heal, M., Heard, D., Hewitt, C. N., Hu, M., Ji, D., Jiang, X., Jones, R., Kalberer, M., Kelly, F. J., Kramer, L., Langford, B., Lin, C., Lewis, A. C., Li, J., Li, W., Liu, H., Loh, M., Lu, K., Mann, G., McFiggans, G., Miller, M., Mills, G., Monk, P., Nemitz, E., O'Connor, F., Ouyang, B., Palmer, P. I., Percival, C., Popoola, O., Reeves, C., Rickard, A. R., Shao, L., Shi, G., 915 Spracklen, D., Stevenson, D., Sun, Y., Sun, Z., Tao, S., Tong, S., Wang, Q., Wang, W., Wang, X., Wang, Z., Whalley, L., Wu, X., Wu, Z., Xie, P., Yang, F., Zhang, Q., Zhang, Y., Zhang, Y., and Zheng, M.: Introduction to Special Issue – In-depth study of air pollution sources and processes within Beijing and its surrounding region (APHH-Beijing), *Atmos. Chem. Phys.*, 19, 7519-7546, <https://doi.org/10.5194/acp-19-7519-2019>, 2019.

920 Stewart, I. D., and Oke, T. R.: Local climate zones for urban temperature studies, *Amer. Meteor. Soc.*, 93, 1879-1900, <https://doi.org/10.1175/BAMS-D-11-00019.1>, 2012.

Stocker, J., Hood, C., Carruthers, D., McHugh, C.: ADMS-Urban: developments in modelling dispersion from the city scale to the local scale, *Int. J. Environ. Pol.*, 50, <https://doi.org/10.1504/IJEP.2012.051202>, 2012.

[Sun, W., Shao, M., Granier, C., Liu, Y., Ye, C. S., Zheng, J. Y.: Long-term trends of anthropogenic SO<sub>2</sub>, NO<sub>x</sub>, CO, and NMVOCs emissions in China, \*Earth's Future\*, 6, 1112-1133 <https://doi.org/10.1029/2018EF000822>, 2018.](#)

925 Tang, G., Zhu, X., Xin, J., Hu, B., Song, T., Sun, Y., Wang, L., Wu, F., Sun, J., Cheng, M., Chao, N., Li, X., Wang, Y.: Modelling study of boundary-layer ozone over northern China – Part II: Responses to emission reductions during the Beijing Olympics, *Atmos. Res.*, 193, 83-93, <https://doi.org/10.1016/j.atmosres.2017.02.014>, 2017.

Tao, J., Zhang, L., Cao, J., and Zhang, R.: A review of current knowledge concerning PM<sub>2.5</sub> chemical composition, aerosol optical properties and their relationships across China, *Atmos. Chem. Phys.*, 17, 9485-9518, <https://doi.org/10.5194/acp-17-9485-2017>, 2017.

930 Tie, X., Zhang, Q., He, H., Cao, J., Han, S., Gao, Y., Li, X., Jia, X C.: A budget analysis of the formation of haze in Beijing, *Atmos. Environ.*, 100, 25-36, <https://doi.org/10.1016/j.atmosenv.2014.10.038>, 2015.

Venkatram, A.: An examination of the Pasquill-Gifford-Turner dispersion scheme, *Atmos. Environ.*, 30, 1283-1290, [https://doi.org/10.1016/1352-2310\(95\)00367-3](https://doi.org/10.1016/1352-2310(95)00367-3), 1996.

935 Wang, X., Westerdahl, D., Chen, L. C., Wu, Y., Hao, J., Pan, X., Guo, X., Zhang, K. M.: Evaluating the air quality impacts of the 2008 Beijing Olympic Games: On-road emission factors and black carbon profiles, *Atmos. Environ.*, 43, 4535-4543, doi:10.1016/j.atmosenv.2009.06.054, 2009.

Wang, X., Westerdahl, D., Wu, Y., pan, X., Zhang, K. M.: On-road emission factor distributions of individual diesel vehicles in and around Beijing, China, *Atmos. Environ.*, 45, 503-513, <https://doi.org/10.1016/j.atmosenv.2010.09.014>, 2011.

940 Wang, K., Jiang, S., Wang, J., Zhou, C., Wang, X., and Lee, X.: Comparing the diurnal and seasonal variabilities of atmospheric and surface urban heat islands based on the Beijing urban meteorological network, *J. Geophys. Res-Atmos*, 122, <https://doi.org/10.1002/2016JD025304>, 2017.

Formatted: Font: (Default) Times New Roman, 10 pt

945 Wang, Y., Bao, S., Wang, S., Hu, Y., Shi, X., Wang, J., Zhao, B., Jiang, J., Zheng, M., Wu, M., Russell, A. G., Wang, Y., and Hao, J.: Local and regional contributions to fine particulate matter in Beijing during heavy haze episodes, *Science of The Total Environment*, 580, 283-296, <https://doi.org/10.1016/j.scitotenv.2016.12.127>, 2017.

Wang, H., Peng, Y., Zhang, X., Liu, H., Zhang, M., Che, H., Cheng, Y., Zheng, Y.: Contributions to the explosive growth of PM<sub>2.5</sub> mass due to aerosol-radiation feedback and decrease in turbulent diffusion during a red alert heavy haze in Beijing-Tianjin-Hebei, China, *Atmos. Chem. Phys.*, 18, 17717-17733, <https://doi.org/10.5194/acp-18-17717-2018>, 2018.

950 [Wang, N., Lyu, X., Deng, X., Huang, X., Jiang, F., Ding, A.: Aggravating O3 pollution due to NOx emission control in eastern China. \*Science of The Total Environment\*, 677, 732-744, https://doi.org/10.1016/j.scitotenv.2019.04.388, 2019.](https://doi.org/10.1016/j.scitotenv.2019.04.388)

Wen, W., He, X., Ma, X., Wei, P., Cheng, S., Wang, X., Liu, L.: Understanding the regional transport contributions of primary and secondary PM<sub>2.5</sub> components over Beijing during a severe pollution episodes, *Aerosol and Air Quality Research*, 18, 1720-1733, doi: 10.4209/aaqr.2017.10.0406, 2018.

955 Wu, B., Shen, X., Cao, X., Yao, Z., Wu, Y.: Characterisation of the chemical composition of PM<sub>2.5</sub> emitted from on-road China III and China IV diesel trucks in Beijing, China, *Science of The Total Environment*, 551-552, 579-589, <https://doi.org/10.1016/j.scitotenv.2016.02.048>, 2016.

Wu, R., Li, J., Hao, Y., Li, Y., Zeng, L., Xie, S.: Evolution process and sources of ambient volatile organic compounds during severe haze event in Beijing, China, *Science of The Total Environment*, 560-561, 62-72, <https://doi.org/10.1016/j.scitotenv.2016.04.030>, 2016.

960 [Xu, J., Yang, W., Han, B., Wang, M., Wang, Z., Zhao, Z., Bai, Z., Vedel, S.: An advanced spatio-temporal model for particulate matter and gaseous pollutants in Beijing, China. \*Atmos. Env.\*, 211, 120-127, https://doi.org/10.1016/j.atmosenv.2019.04.011, 2019.](https://doi.org/10.1016/j.atmosenv.2019.04.011)

[Xu, M., Sbihi, H., Pan, X., Brauer, M.: Local variation of PM<sub>2.5</sub> and NO<sub>2</sub> concentrations within metropolitan Beijing. \*Atmos. Env.\*, 200, 254-263, https://doi.org/10.1016/j.atmosenv.2018.12.014, 2019.](https://doi.org/10.1016/j.atmosenv.2018.12.014)

965 Yang, G., Wang, Y., Zeng, Y., Gao, G. F., Liang, X., Zhou, M., Wan, X., Yu, S., Jiang, Y., Naghavi, M., Vos, T., Wang, H., Lopez, A. D., Murray, C. J.: Rapid health transition in China, 1990-2010: findings from the Global Burden of Disease Study 2010, *The Lancet*, 381, 1987-2015, [https://doi.org/10.1016/S0140-6736\(13\)61097-1](https://doi.org/10.1016/S0140-6736(13)61097-1), 2013.

970 Yang, D., Zhang, S., Niu, T., Wang, Y., Xu, H., Zhang, K. M., Wu, Y.: High-resolution mapping of vehicle emissions of atmospheric pollutants based on large-scale, real-world traffic datasets, *Atmos. Chem. Phys. Discuss.*, <https://doi.org/10.5194/acp-2019-32>, 2019.

Zhang, S., Wu, Y., Wu, X., Li, M., Ge, Y., Liang, B., Xu, Y., Zhou, Y., Liu, H., Fu, L., and Hao, J.: Historic and future trends of vehicle emissions in Beijing, 1998-2020: A policy assessment for the most stringent vehicle emission control program in China, *Atmos. Environ.*, 89, 216-229, <https://doi.org/10.1016/j.atmosenv.2013.12.002>, 2014.

975 Zhang, Y., Yao, Z., Shen, X., Liu, H., He, K.: Chemical characterization of PM<sub>2.5</sub> emitted from on-road heavy-duty diesel trucks in China, *Atmos. Environ.*, 122, 885-891, <https://doi.org/10.1016/j.atmosenv.2015.07.014>, 2015.

Zhang, L., Liu, L., Zhao, Y., Gong, S., Zhang, X., Henze, D. K., Capps, S. L., Fu, T.-M., Zhang, Q., Wang, Y.: Source attribution of particulate matter pollution over North China with the adjoint method, *Environ. Res. Lett.*, 10, doi:10.1088/1748-9326/10/8/084011, 2015.

980 Zhang, Z., Zhang, X., Gong, D., Kim, S.-J., Mao, R., Zhao, X.: Possible influence of atmospheric circulations on winter haze pollution in the Beijing-Tianjin-Hebei region, northern China, *Atmos. Chem. Phys.*, 16, 561-571, <https://doi.org/10.5194/acp-16-561-2016>, 2016.

Zhang, X., Zhong, J., Wang, J., Wang, Y., Liu, Y.: The interdecadal worsening of weather conditions affecting aerosol pollution in the Beijing area in relation to climate warming, *Atmos. Chem. Phys.*, 18, 5991-5999, <https://doi.org/10.5194/acp-18-5991-2018>, 2018.

985

Formatted: Font: (Default) Times New Roman, 10 pt

Formatted: English (United Kingdom)

Formatted: Default Paragraph Font

Formatted: Font: (Default) Times New Roman, 10 pt

Zhang, Y., Andre, M., Liu, Y., Wu, L., Jing, B., Mao, H.: Evaluation of low emission zone policy on vehicle emission reduction in Beijing, China, *IOP Conf. Ser.: Earth Environ. Sci.*, 121, doi:10.1088/1755-1315/121/5/0520702018, 2018.

Zhang, S., Wu, Y., Yan, H., Du, X., Zhang, K. M., Zheng, X., Fu, L., Hao, J.: Black carbon pollution for a major road in Beijing: Implications for policy interventions of the heavy-duty truck fleet, *Trans. Res. Part D: Trans. Environ.*, 68, 110-121, <https://doi.org/10.1016/j.trd.2017.07.013>, 2019.

Zheng, B., Huo, H., Zhang, Q., Yao, Z. L., Wang, X. T., Yang, X. F., Liu, H., and He, K. B.: High-resolution mapping of vehicle emissions in China in 2008, *Atmos. Chem. Phys.*, 14, 9787-9805, <https://doi.org/10.5194/acp-14-9787-2014>, 2014.

Zheng, G. J., Duan, F. K., Su, H., Ma, Y. L., Cheng, Y., Zheng, B., Zhang, Q., Huang, T., Kimoto, T., Chang, D., Poschl, U., Cheng, Y. F., He, K. B.: Exploring the severe winter haze in Beijing: the impact of synoptic weather, regional transport and heterogeneous reactions, *Atmos. Chem. Phys.*, 15, 2969-2983, <https://doi.org/10.5194/acp-15-2969-2015>, 2015.

Zheng, B., Zhang, Q., Tong, D., Chen, C., Hong, C., Li, M., Geng, G., Lei, Y., Huo, H., He, K.: Resolution dependence of uncertainties in gridded emission inventories: a case study in Hebei, China, *Atmos. Chem. Phys.*, 17 921-933, doi:10.5194/acp-17-921-2017, 2017.

Zheng, B., Tong, D., Li, M., Liu, F., Hong, C., Geng, G., Li, H., Li, X., Peng, L., Qi, J., Yan, L., Zhang, Y., Zhao, H., Zheng, Y., He, K., Zhang, Q.: Trends in China's anthropogenic emissions since 2010 as the consequence of clean air actions, *Atmos. Chem. Phys.*, 18, 14095-14111, <https://doi.org/10.5194/acp-18-14095-2018>, 2018.

Zhong, M., Saikawa, E., Liu, Y., Naik, V., Horowitz, L. W., Takigawa, M., Zhao, Y., Lin, N-H., Stone, E. A.: Air quality modelling with WRF-Chem v3.5 in East Asia: sensitivity to emissions and evaluation of simulated air quality, *Geosci. Model. Dev.*, 9, 1201-1218, <https://doi.org/10.5194/gmd-9-1201-2016>, 2016.

Zhou, J., Chen, Y., Zhang, X., Zhan, W.: Modelling the diurnal variations of urban heat islands with multi-source satellite data, *International Journal of Remote Sensing*, 34, 7568-7588, <https://doi.org/10.1080/01431161.2013.821576>, 2013.

Formatted: Font: (Default) Times New Roman, 10 pt

Formatted: Font: 10 pt

1025

1030

1035

1040

1045

1050

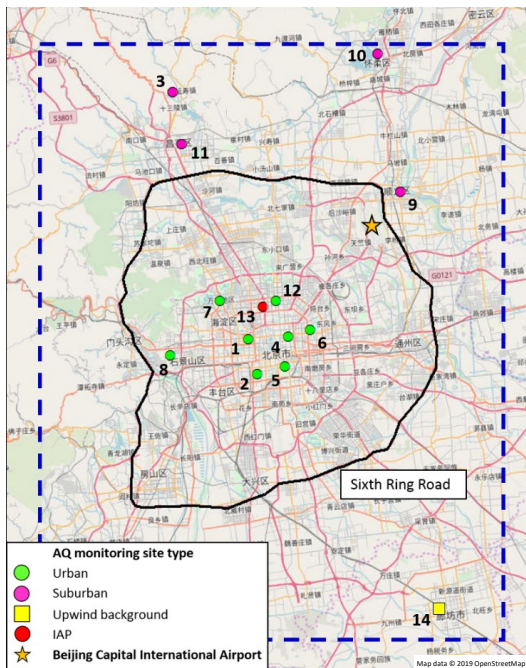


Figure 1: Map of Beijing (source: OpenStreetMap) with modelling domain, measuring 75 km x 90 km, outlined (dashed blue line). Urban (green circle), suburban (pink circle), upwind background (yellow square) and IAP (red circle) air quality monitoring station locations, including site numbers, are provided. Beijing Capital International Airport (yellow star) and the Sixth Ring Road (black line) are also highlighted.

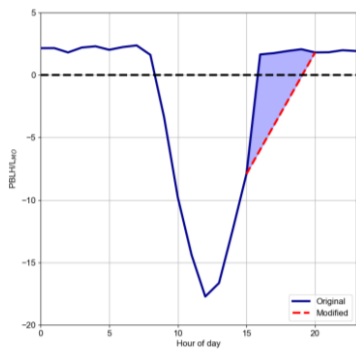


Figure 2: Diurnal mean PBLH/LMO values for the campaign period (blue line). Modified PBLH/LMO, from 4-7pm, to account for evening UHI, shown by red dashed line.

1055

1060

1065

1070

1075

1080

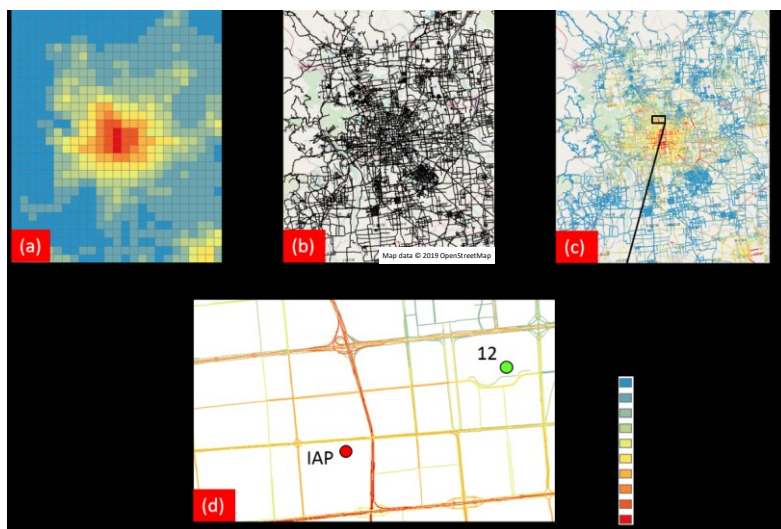
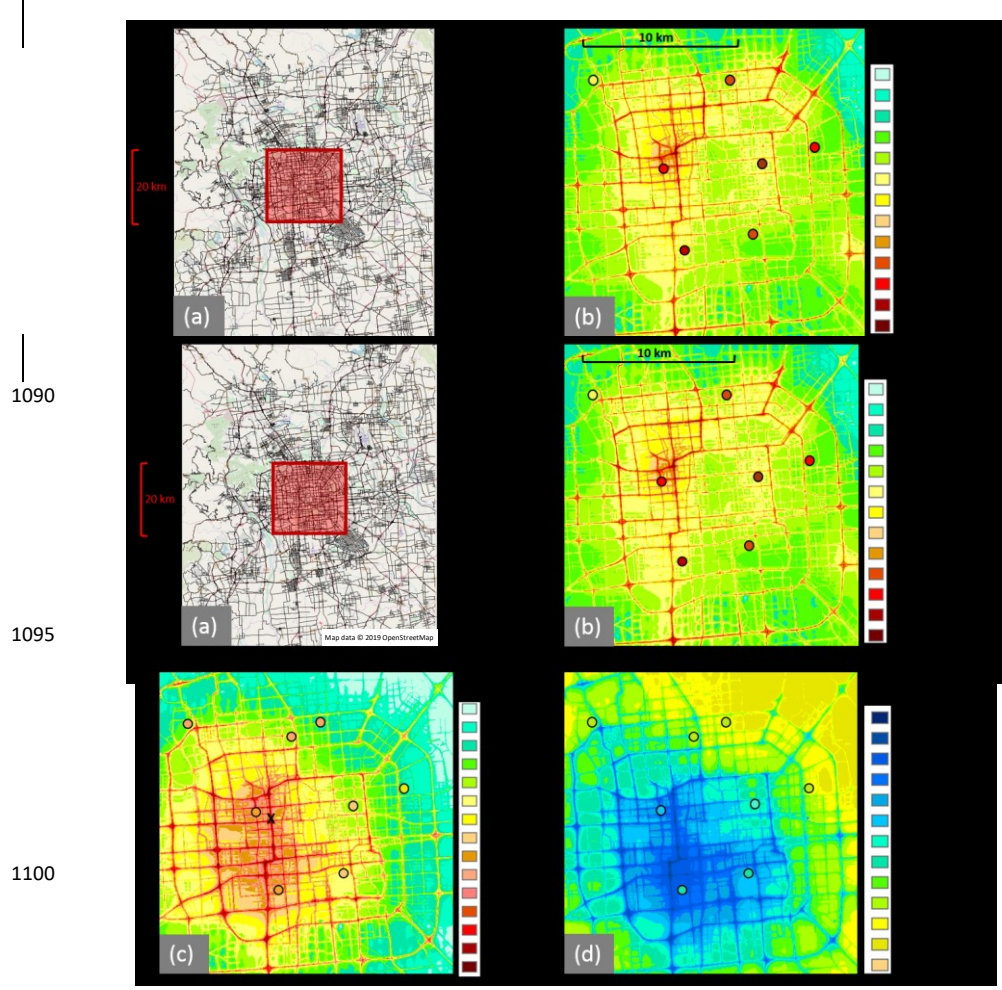


Figure 33: (a) Spatial distribution of November and December mean transportation sector MEIC Std NO<sub>2</sub> emissions (lowest vertical layer) covering full study domain, (b) Spatial road network of Beijing (source: OpenStreetMap), (c) explicit road source NO<sub>2</sub> emission rates following apportioning of (a) onto (b), and (d) enlarged Sect. of road emissions network covering the IAP field site and site 12.



1090

1095

1100

1105

Figure 4: Spatial maps of mean PM<sub>2.5</sub> (b), NO<sub>2</sub> (c), and O<sub>3</sub> (d) concentrations for the winter campaign period (5/11/16 to 10/12/16), simulated using the MEIC Opt emissions inventory. Simulated concentrations cover the region marked in (a). Mean measured concentrations at monitoring network sites (NO<sub>2</sub>, O<sub>3</sub> and PM<sub>2.5</sub>) and the IAP field site (NO<sub>2</sub> and O<sub>3</sub>) are represented by coloured dots.

1110

1115

1120

1125

1130

1135

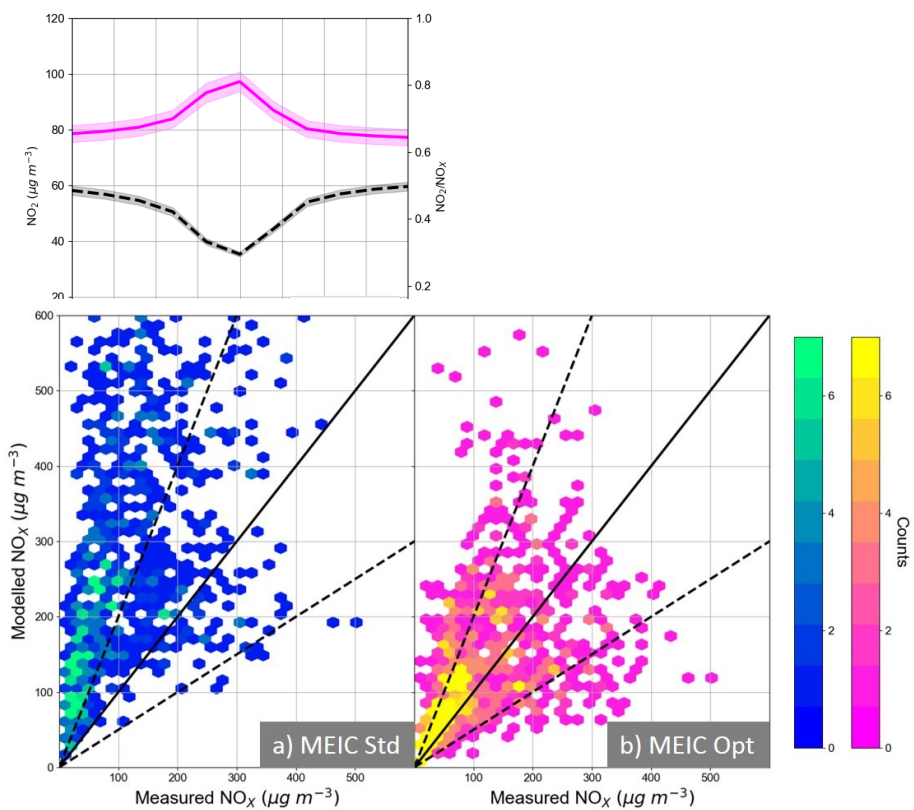


Figure 6: Hourly measured and modelled  $\text{NO}_x$  concentrations during the campaign period at the IAP field site. Panel (a) and (b) showing concentrations simulated using MEIC Std and MEIC Opt, respectively. Colours represent the total number of matching hourly measured and modelled values contained within distinct hexagonal bins. Dashed lines mark factor of two difference between measured and simulated concentrations.

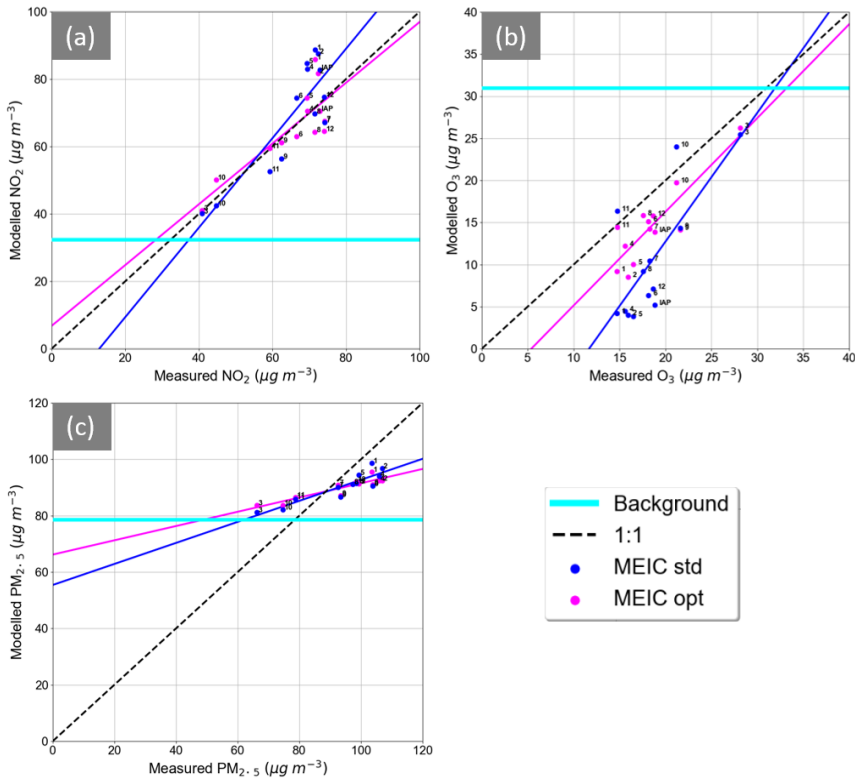


Figure 7: Campaign period mean measured and modelled (a) NO<sub>2</sub>, (b) O<sub>3</sub>, and (c) PM<sub>2.5</sub> concentrations at all monitoring network sites (numbered) and the IAP field site (NO<sub>2</sub> and O<sub>3</sub>). Blue and pink lines indicate concentrations simulated using MEIC Std and MEIC Opt, respectively. Horizontal light blue line represents campaign period mean background concentrations calculated from measurements.

Formatted: Tab stops: 1.81 cm, Left

1170

1175

1180

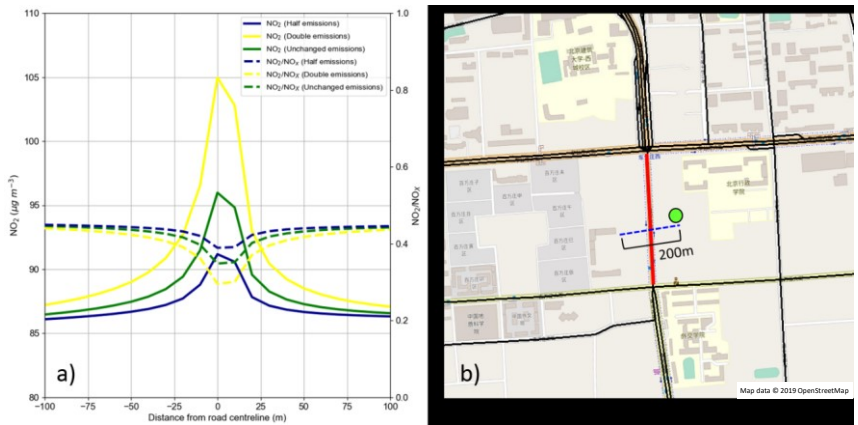


Figure 8: (a) Campaign period mean simulated NO<sub>2</sub> concentrations and NO<sub>2</sub>/NO<sub>x</sub> concentration ratios with distance from road centre along cross-road slice marked in (b) using half (blue), double (yellow) and unchanged (green) emissions of all species from explicit road source marked by red line. Green circle in (b) marks position of monitoring site 1.

1185

1190

1195

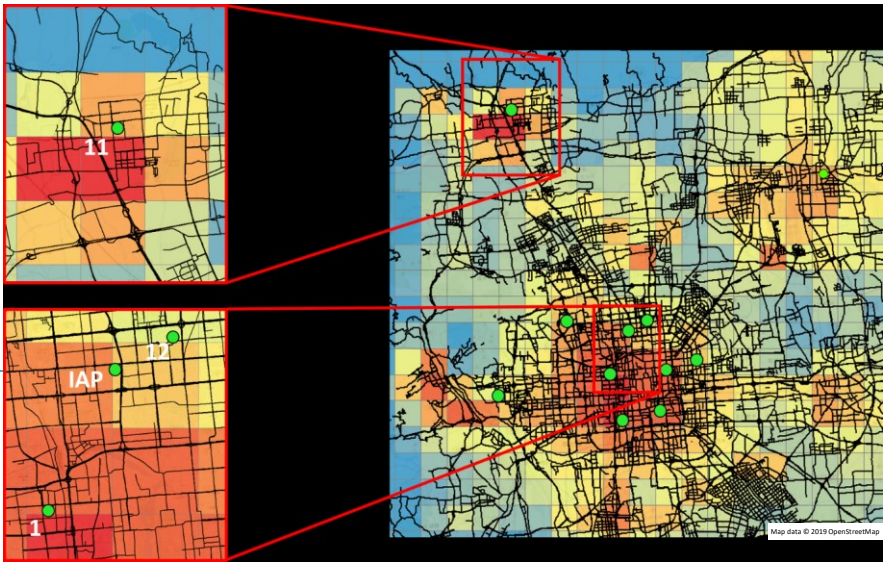


Figure 9: Spatial distribution of November and December mean MEIC Opt NO<sub>2</sub> emissions (all emission sectors) overlaid with Beijing road network (source: OpenStreetMap). Enlarged regions cover urban sites 1, 12 and IAP as well as suburban site 11.

1200

1205

1210

1215

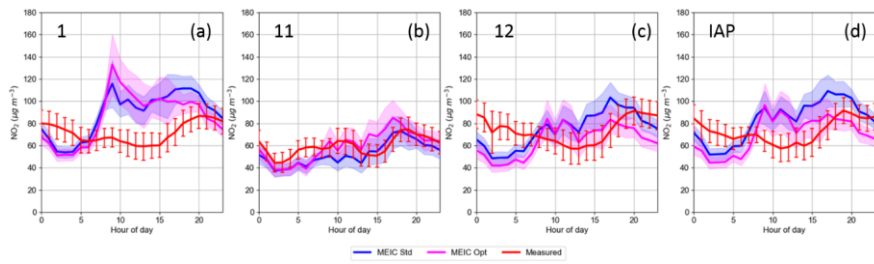


**Figure 10: Campaign period mean diurnal variation in modelled and measured NO<sub>2</sub> concentrations at sites (a) 1, (b) 11, (c) 12, and (d) IAP. Modelled concentrations produced using both MEIC Std (blue) and MEIC Opt (pink). Measurements marked by red line. Shaded areas and error bars represent the 95% confidence intervals for simulated and measured concentrations, respectively.**

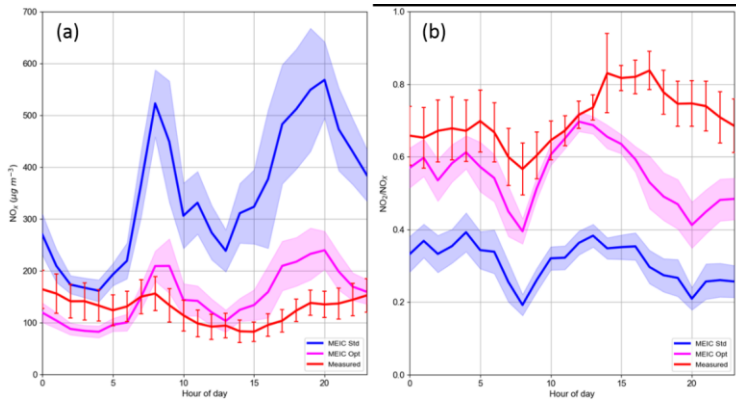


Figure 11: Campaign period mean diurnal variation in modelled and measured (a)  $\text{NO}_x$  concentrations and (b)  $\text{NO}_2/\text{NO}_x$  concentration ratios at the IAP field site. Modelled concentrations produced using both MEIC Std (blue) and MEIC Opt (pink). Measurements marked by red line. Shaded areas and error bars represent the 95% confidence intervals for simulated and measured concentrations, respectively.

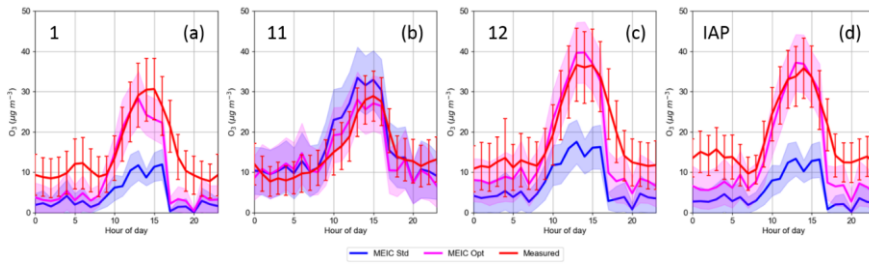
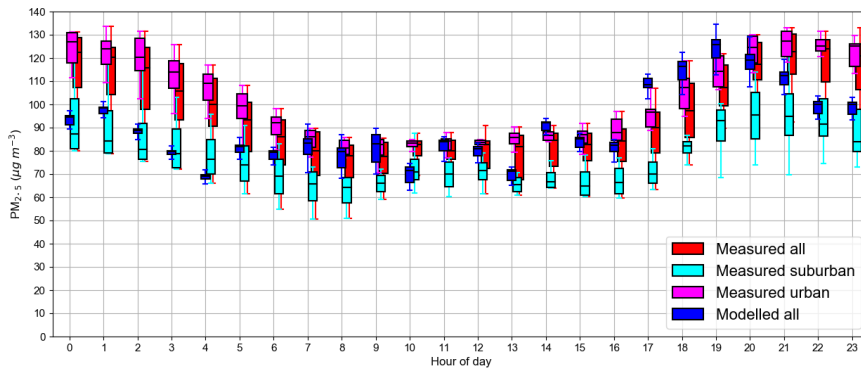


Figure 12: Campaign period mean diurnal variation in modelled and measured  $\text{O}_3$  concentrations at sites (a) 1, (b) 11, (c) 12 and (d) IAP. Modelled concentrations produced using both MEIC Std (blue) and MEIC Opt (pink). Measurements marked by red line. Shaded areas and error bars represent the 95% confidence intervals for simulated and measured concentrations, respectively.

1240



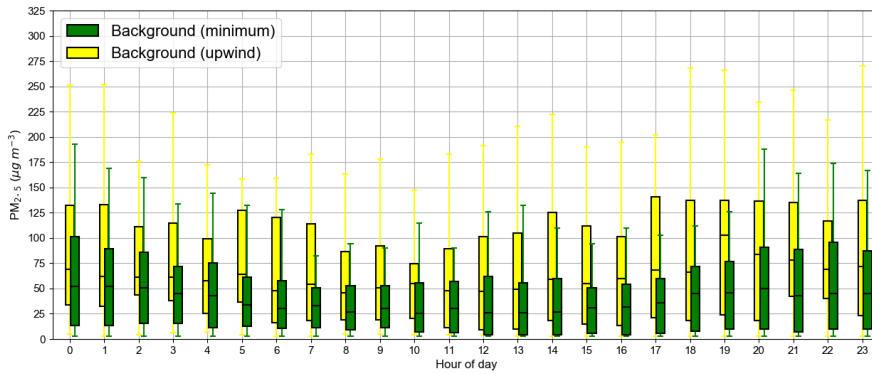
1245

Figure 13: Variations in site-specific campaign period mean measured (red) and modelled (blue) PM<sub>2.5</sub> concentrations across all monitoring network stations for each hour of the day. Measurements sub-divided to highlight the variation between suburban (cyan) and urban (pink) monitoring network stations specifically.

1250

1255

1260



1265

Figure 14: Ranges in campaign period mean calculated background PM<sub>2.5</sub> concentrations for each hour of the day using minimum (green) and upwind (yellow) concentration methodologies.

1270

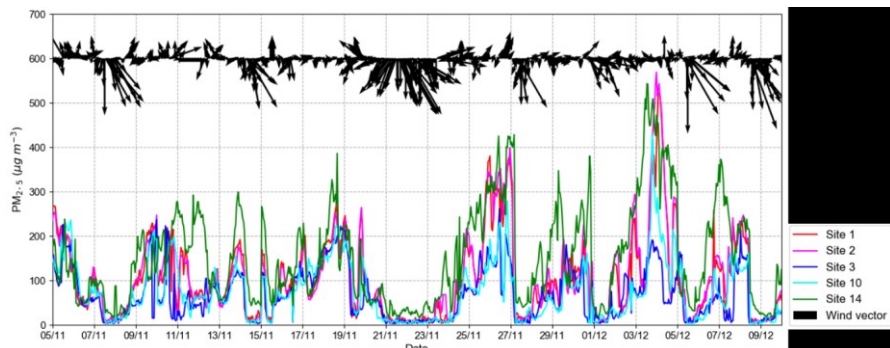


Figure 15: Hourly PM<sub>2.5</sub> concentrations at measurement sites 1, 2, 3, 10 and 14 during the campaign period. Wind vectors, representing wind speed magnitude and direction recorded at the airport meteorological station, are also provided (black arrows).

1275

1280

1285

1290

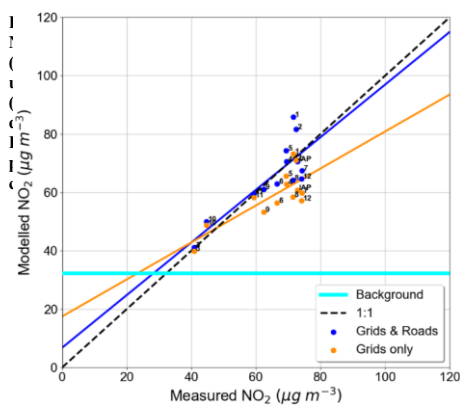


Figure 16: Campaign period measured and modelled NO<sub>2</sub> concentrations at all measurement sites (numbered). Modelled concentrations produced using 3-D grid and explicit road emission sources (blue), and 3-D grid sources only (orange/green) derived from the MEIC Opt emissions inventory. Horizontal light blue line represents campaign period mean background NO<sub>2</sub> concentrations calculated from measurements.

1295

1300

1305

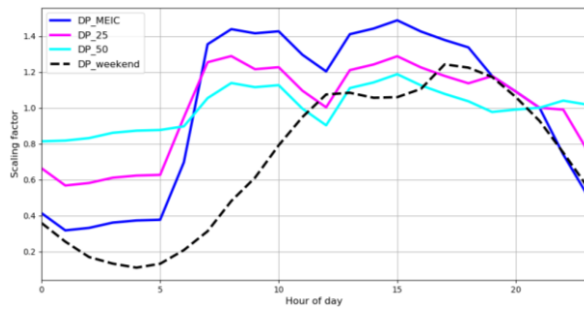
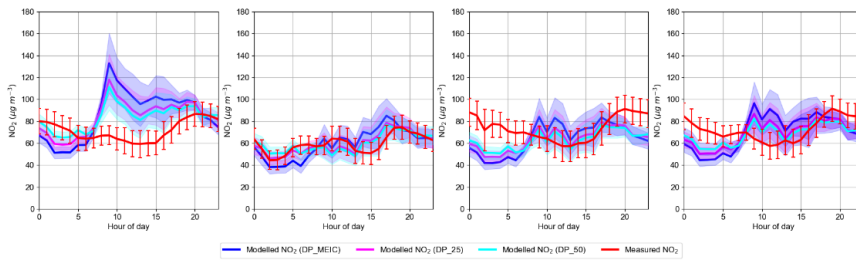


Figure 17: Diurnal emissions profiles applied to the simulations shown in Fig. 18. Standard MEIC diurnal emissions profile (DP\_MEIC) marked by blue line; modified DP\_MEIC with increased proportions of nighttime emissions marked by pink (DP\_25) and cyan (DP\_50) lines and weekend emissions profile marked by dashed black line.

1310

1315



1320

Figure 18: Campaign period mean diurnal variation in measured and modelled NO<sub>2</sub> concentrations using MEIC Opt at sites (a) 1, (b) 11, (c) 12, and (d) IAP. Measurements marked by red line. Shaded areas and error bars represent the 95% confidence intervals for simulated and measured concentrations, respectively.

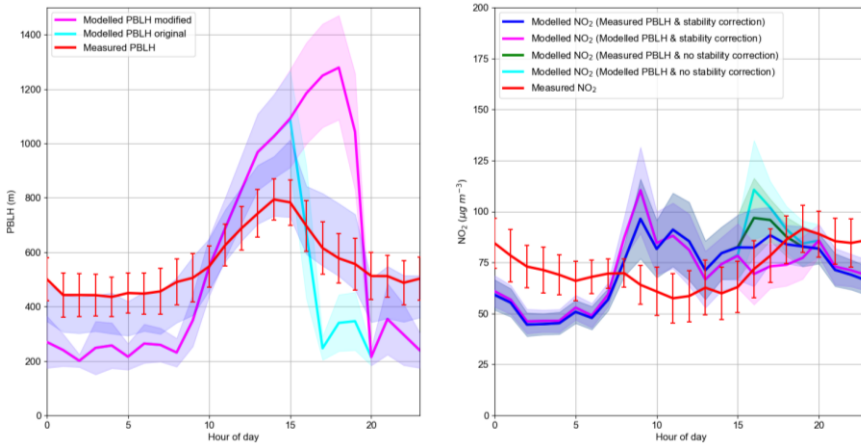


**Figure 19: (a) Campaign period mean diurnal variation in modelled PBLH with stability correction (pink), modelled PBLH without stability correction (cyan) and measured PBLH (red). (b) Campaign period mean diurnal variation in measured (red) and modelled NO<sub>2</sub> concentrations with measured PBLH and stability correction (blue), modelled PBLH with stability correction (pink), measured PBLH without stability correction (green), and modelled PBLH without stability correction (cyan) at the IAP field site. Shaded areas and error bars represent the 95% confidence intervals for simulated and measured PBLH and concentrations, respectively.**

1325

1330

**Table 1: Locations (latitude and longitude) of all monitoring stations, including distinction between urban (within sixth ring road) and suburban site types. Approximate distance (nearest 10 m) from each monitoring station to nearest road centreline and corresponding road type also provided.**

1335

Site name	Site type	Latitude (°N)	Longitude (°E)	Distance to nearest road centreline (m)	Nearest Road type
-----------	-----------	---------------	----------------	---	-------------------

1	Guanyuan	Urban	39.93	116.34	90	Secondary
2	Wanshou Xigong	Urban	39.88	116.35	80	Tertiary
3	Dingling	Suburban	40.29	116.22	285	Tertiary
4	Dongsi	Urban	39.93	116.42	200	Secondary
5	Tiantan	Urban	39.89	116.41	90	Tertiary
6	Nongzhanguan	Urban	39.94	116.46	400	Trunk
7	Haidan Wanliu	Urban	39.99	116.29	100	Tertiary
8	Gucheng	Urban	39.91	116.18	260	Tertiary
9	Shunyicheng	Suburban	40.13	116.66	190	Secondary
10	Huairouzhen	Suburban	40.33	116.63	N/A	Tertiary
11	Changpingzhen	Suburban	40.22	116.23	200	Secondary
12	Aoti Zhongxin (Olympic Park)	Urban	39.98	116.4	110	Secondary
13	IAP	Urban	39.97	116.37	110	Secondary
14	TCM Medical Material Company	Urban	39.52	116.69	N/A	Secondary

1340

Table 2: Campaign period mean MEIC Std (S) and MEIC Opt (O) pollutant species emissions (Tonnes day<sup>-1</sup>) aggregated across all, urban and suburban grid cells. Change (%) in emissions between inventories, following optimisation, calculated as (O – S/S) x 100.

1345

Campaign period mean aggregate pollutant emission rates (Tonnes day <sup>-1</sup> )												
Region of domain	NO <sub>2</sub>		NO <sub>x</sub>		PM <sub>2.5</sub>		PM <sub>10</sub>		SO <sub>2</sub>		VOC	
	S	O	S	O	S	O	S	O	S	O	S	O
All	60.3	46.8	889.3	504.8	86.3	110.3	156.5	176.4	72.5	54.4	717.6	1942.8
Change (%)	-22.1		-43.3		28.0		12.5		-25.0		170.7	
Urban	44.0	22.1	649.1	238.3	49.9	28.0	46.9	89.3	22.5	69.5	426.8	1273.1
Change (%)	-49.8		-63.3		-6.0		-22.2		-35.1		167.0	
Suburban	16.3	24.7	240.2	266.2	36.3	6.0	63.4	67.2	27.0	106.7	240.8	669.4
Change (%)	51.5		10.8		74.7		58.8		-10.3		178.0	

- Formatted Table

1350 Table 3: Estimated emission weighting factors for each modelled road type.

Road Type	Weighting
Motorway	0.7
Trunk	0.5
Primary	0.4
Secondary	0.25
Tertiary	0.15

1355

Table 4: Statistical evaluation of modelled pollutant concentrations for the campaign period, using MEIC Std (S) and MEIC Opt (O) emissions inventories. Mean modelled (Mod) and observed (Obs) concentrations and statistics divided into all (12 monitoring network sites and IAP field site for NO<sub>2</sub> and O<sub>3</sub>, monitoring network sites only for PM<sub>2.5</sub>) and urban and suburban monitoring site groups. Urban and suburban sites defined in Table 1. NO<sub>x</sub> measurements only available at the IAP field site. Mean concentrations and statistics calculated from matching hourly values.

	Sites	Mean Concentrations (µg m <sup>-3</sup> )			Model Evaluation Statistics					
		Mod (S)	Mod (O)	Obs	NMSE		Fb		R	
					S	O	S	O	S	O
PM <sub>2.5</sub>	All	90.3	89.8	93.4	0.37	0.37	-0.03	-0.04	0.76	0.76
	Urb	93.4	92.1	100.9	0.36	0.36	-0.08	-0.09	0.78	0.78
	Sub	84.0	85.3	78.3	0.40	0.41	0.07	0.09	0.74	0.74
O <sub>3</sub>	All	10.4	14.6	18.5	1.54	0.74	-0.56	-0.24	0.71	0.79
	Urb	6.1	12.8	17.2	3.20	0.93	-0.95	-0.29	0.70	0.77
	Sub	20.0	18.6	21.4	0.48	0.47	-0.07	-0.14	0.82	0.83
NO <sub>2</sub>	All	69.5	65.7	65.3	0.27	0.30	0.06	0.00	0.55	0.53
	Urb	79.2	71.4	71.3	0.27	0.31	0.10	0.00	0.42	0.44
	Sub	47.9	52.9	51.8	0.21	0.23	-0.08	0.02	0.74	0.70
NO <sub>x</sub>	IAP	345.5	149.8	126.1	2.35	0.63	0.93	0.17	0.35	0.41

Formatted: Position: Vertical: 0.05 cm, Relative to: Paragraph

Formatted: Position: Horizontal: 7.72 cm, Relative to: Page, Vertical: 0.44 cm, Relative to: Paragraph

Formatted: Position: Horizontal: 7.72 cm, Relative to: Page, Vertical: 0.44 cm, Relative to: Paragraph

Formatted: Position: Horizontal: 7.72 cm, Relative to: Page, Vertical: 0.44 cm, Relative to: Paragraph

Formatted: Position: Horizontal: 7.72 cm, Relative to: Page, Vertical: 0.44 cm, Relative to: Paragraph

Formatted: Position: Horizontal: 7.72 cm, Relative to: Page, Vertical: 0.44 cm, Relative to: Paragraph

Formatted: Position: Horizontal: 7.72 cm, Relative to: Page, Vertical: 0.44 cm, Relative to: Paragraph

Formatted: Position: Horizontal: 7.72 cm, Relative to: Page, Vertical: 0.44 cm, Relative to: Paragraph

	Site	Mean Concentrations (µg m <sup>-3</sup> )			Model Evaluation Statistics					
		Mod (G)	Mod (G-R)	Obs	NMSE		Fb		R	
					G	G-R	G	G-R	G	G-R
NO <sub>2</sub>	All	58.9	65.7	65.3	0.28	0.30	-0.10	0.00	0.59	0.53
	Urb	62.8	71.4	71.3	0.29	0.31	-0.13	0.00	0.51	0.44
	Sub	50.1	52.9	51.8	0.21	0.23	-0.03	0.02	0.73	0.70

1360

Table 5: Same information presented as in Table 4 but for NO<sub>2</sub> concentrations simulated (MEIC Opt) using 3-D grid sources only (G) as well as 3-D grid and explicit road sources (G-R) (also presented in Table 4).

Formatted: Position: Horizontal: 2.78 cm, Relative to: Page, Vertical: 0.08 cm, Relative to: Paragraph

1365

We thank both reviewers for their detailed and insightful feedback on this study which has considerably improved the manuscript. Responses to each comment are structured as follows: (a) reviewer comment (in bold), (b) our response to the comment, (c) changes to the manuscript (in quotation marks and italics). In the revised manuscript modified text is highlighted using Track Changes.

**Referee #1**

**In this manuscript, the authors use the Gaussian pollution dispersion and chemistry model named ADMS-Urban simulating the street-scale resolution concentrations of NO<sub>x</sub>, NO<sub>2</sub>, O<sub>3</sub> and PM<sub>2.5</sub> in Beijing. They construct a traffic emissions inventory, and this method improves the consistency of simulation data and measurement data of Beijing's air quality monitoring network and the Institute of Atmospheric Physics (IAP) field site. ADMS-Urban model can solve the sharp concentration gradients adjacent to major roads. This manuscript can provide valuable information for evaluating the street-scale air quality. The following advices hope to attract your attention.**

We thank the reviewer for their positive feedback.

**1. Several articles have been quoted many times in the introduction. It is recommended that multiple references be cited to reflect the amount of reading and to enhance the persuasion.**

We thank the reviewer for this comment as we agree some articles have been cited on a number of occasions. To address this, the following references have been added throughout the introduction to help explain key points:

On Page 2 Line 55 studies by Li et al. (2018) and Cui et al. (2019) are cited in which data from Beijing's air quality monitoring network is extensively analysed. Cheng et al. (2019) has been removed as it is more relevant to emission reduction estimates in Beijing discussed in the following paragraph, in which it is referenced multiple times. In the subsequent paragraph on Line 63 a reference to Sun et al. (2018), who investigated China's emission trends, has been added. On Line 65 articles by Ni et al. (2018) and Wang et al. (2019) are included in which the impacts of China's extensive implementation of emission control techniques are discussed.

As described in detail in response to reviewer comment 3, on Page 3 Line 86 and 89 recent studies describing alternative urban air quality modelling techniques are added – J. Xu et al. (2019), M. Xu et al. (2019) and Lugon et al. (2019). Page 2/3 Line 84-89 now reads:

*“Land use regression (LUR) modelling studies, combining geospatial indicators with air quality measurement data, can generate local scale (<1 km) pollutant level variations, but have been limited by the sparsity of monitoring network data available in Beijing (J. Xu et al. 2019; M. Xu et al. 2019). Alternatively, box models, such as The Model of Urban Network of Intersecting Canyons and Highways (MUNICH), are used to calculate pollutant concentrations within street canyons, but require detailed information on the spatial dimensions of a city's street canyons and are restricted by assumptions of uniform concentrations along individual road segments (Lugon et al. 2019).”*

On Line 106 a further study (Zhang et al. 2018) describing a recently constructed bottom-up road traffic emissions inventory for Beijing is cited. Page 3 Line 106-108 of the updated manuscript:

*“A bottom-up street-scale vehicle emissions inventory was also created by Zhang et al. (2018), using traffic surveys and video identification of vehicle fleet composition to evaluate the impact of a new low emission zone (LEZ) in urban Beijing.”*

**2. The novelty of this work should be highlighted in the introduction. I suggest present in the last two paragraph.**

We thank the reviewer for this comment. We have now highlighted the novelty of this work in relation to both the methodology for generating the road emissions network, which can be applied to urban areas elsewhere with limited data availability, and the evaluation of street-scale modelled concentrations using measurements from

1410 both Beijing's air quality monitoring network and an intensive measurement campaign. Page 3 Line 111-113 of the updated manuscript:

*"However, this work provides a robust framework suitable for similar street-scale air quality modelling across large urban areas with limited data availability that future human health studies can build on."*

Page 3 Line 118-120 of the updated manuscript:

1415 *"Measured pollutant concentrations from both the APHH-China campaign and Beijing's air quality monitoring network are used to evaluate modelled concentrations, providing valuable insight into the key processes that impact street-scale air quality."*

The suitability of ADMS-Urban for performing sensitivity studies that further explore the discrepancies between modelled and measured concentrations is also highlighted on Page 3 Line 120:

1420 *"The adaptability of ADMS-urban is utilised in a series of further sensitivity simulations aimed at exploring the impact that..."*

**3. The introduction is long and unclear. You should summarize the advantages and disadvantages of various methods at the end to highlight your innovation points of the article.**

We thank the reviewer for this comment. We have now summarised the advantages and disadvantages of various methods by outlining both land use regression (LUR) and box model approaches to urban air quality modelling, with limitations of both highlighted.

1425 The manuscript has been updated on Page 2 from Line 83:

*"...As a result, a range of street-scale resolution air quality modelling techniques have recently emerged. Land use regression (LUR) modelling studies, combining geospatial indicators with air quality measurement data, can generate local scale (<1 km) pollutant level variations, but have been limited by the sparsity of monitoring network data available in Beijing (J. Xu et al. 2019; M. Xu et al. 2019). Alternatively, box models, such as The Model of Urban Network of Intersecting Canyons and Highways (MUNICH), are used to calculate pollutant concentrations within street canyons, but require detailed information on the spatial dimensions of a city's street canyons and are restricted by assumptions of uniform concentrations along individual road segments (Lugon et al. 2019)."*

1430 Distinction between ADMS-Urban and the US EPA's environmental regulatory model AERMOD has been added with ADMS-Urban's use of a simplified chemistry scheme explicitly stated on Page 3 Line 93:

*"The additional modelling of local fast chemistry processes on pollutant emissions with ADMS-Urban, involving the simplified Generic Reaction Set (GRS) chemistry scheme, including NO<sub>x</sub>-O<sub>3</sub> reactions, enables sharp concentration gradients adjacent to major urban sources to be captured (Hood et al. 2018)."*

1440 As outlined above in response to reviewer 1 comment 1, on Line 107 an additional study by Zhang et al. (2018) is cited in which the impacts of a recently introduced low emission zone (LEZ) in urban Beijing on a newly constructed bottom-up street-scale road traffic emissions inventory are investigated. On Line 106-108 of the updated manuscript:

1445 *"A bottom-up street-scale vehicle emissions inventory was also created by Zhang et al. (2018), using traffic surveys and video identification of vehicle fleet composition to evaluate the impact of a new low emission zone (LEZ) in urban Beijing."*

The disadvantages of the methodology adopted here for generating the explicit network of road emissions compared with the Zhang et al. (2018) and Yang et al. (2019) studies have been outlined on Page 3 Line 110:

1450 “Unlike the data-intensive methodology adopted by Yang et al. (2019), spatiotemporal variations in traffic volume and vehicle type are not considered here.”

However, the advantage of apportioning coarser resolution gridded emissions onto the openly available OpenStreetmap (OSM) spatial road network compared with the data-intensive Zhang et al. (2018) and Yang et al. (2019) techniques is highlighted on Page 3 Line 111:

1455 “...However, this work provides a robust framework suitable for similar street-scale air quality modelling across large urban areas with limited data availability that future human health studies can build on.”

The reviewer also commented on the introduction’s excessive length. To address this, the previously detailed summaries of numerous regional modelling studies in Beijing have been removed. Page 2 Lines 80-82 of the updated manuscript:

1460 “Numerous regional modelling studies, incorporating emission inventories such as MEIC and Eulerian chemical transport models (CTMs), have been carried out for Beijing (Liu et al. 2016; Petaja et al. 2016; Li et al. 2017; Wang et al. 2017; Wang et al. 2018; Chang et al. 2019).”

Descriptions of earlier urban air quality modelling studies using ADMS-Urban in other countries have also been removed from Page 3 in order to allow for greater focus on the advantages and disadvantages of distinctly

1465 different approaches to urban air quality modelling and road traffic emission inventory construction.

**4. Line 134, don’t quote the two references separately, insert them at the end of the sentence.**

As suggested, both references have been moved to the end of the sentence.

Page 4 Line 135-138 of the manuscript:

1470 “ADMS-Urban, developed by Cambridge Environmental Research Consultants (CERC), is a quasi-Gaussian pollution dispersion and chemistry model that has been applied worldwide for environmental regulation, investigation and assessment of emission control strategies and generation of high spatial resolution air quality forecasts (McHugh et al. 2005; Carruthers, 2009; Cai and Xie, 2011).”

**5. Line 144, please explain the reason for using hourly wind direction and speed.**

1475 Hourly values of all meteorological variables (wind speed, wind direction, air temperature and cloud cover ) are used to drive hourly plume dispersion calculations. Parameters determining the stability of the PBL ( $F_{00}$ ,  $U^*$  and  $L_{MO}$ ) are calculated for each hour using the input meteorology. These parameters are subsequently used in the model to calculate horizontal and vertical plume spread parameters that determine hourly pollutant concentrations via Gaussian distribution equations and the summation of contributions from individual emission sources.

1480 To clarify that all input meteorological variables used are hourly-varying, Page 4 Line 146 of the manuscript is updated to:

“For this study, we use hourly wind speed, wind direction, air temperature and cloud cover data from the Beijing Capital International Airport Meteorology Observatory...”

Line 160-162 of the updated manuscript:

1485 “This  $PBLH/L_{MO}$  parameterisation controls the vertical and horizontal spread extents of each emitted Gaussian plume, with the aggregate contribution from each individual emission source determining hourly simulated pollutant concentrations.”

**6. Lines 229-231, data should be provided to support this point.**

The manuscript has been updated to explicitly state the monitoring stations used to estimate background  $PM_{2.5}$  and  $PM_{10}$  concentrations as well as the wind directions associated with each.

1490 Page 6 Line 234-236:

*“For particulate matter ( $PM_{2.5}$  and  $PM_{10}$ ), an hourly upwind background concentration is derived based on wind direction with concentrations selected from sites 3 (270-360°), 10 (0-90°) and 14 (90-270°) located to the NW, NE and SE of urban Beijing, respectively.”*

1495 **7. It is suggested that Sect. 3.3 should focus on the comparison of the simulation results using the MEIC Std and MEIC Opt emission inventories. On this basis, the specific conclusions are explained.**

We thank the reviewer for this comment, however the exact nature of the recommended changes is unclear. Both Sect. 3.2 and 3.3 present comparisons of simulation results using the MEIC Std and MEIC Opt inventories, however with different objectives. Through the statistical evaluation of site-specific period mean measured and simulated concentrations, the primary aims of Sect. 3.2 are to demonstrate overall model performance as well as the impact of the redistribution and magnitude adjustment of emissions with MEIC Opt on the spatial variation of simulated pollutant concentrations. Clear improvements in model performance using MEIC Opt for all pollutant species highlight issues with using spatial proxy-based emission inventories for street-scale air quality modelling. In Sect. 3.3 the focus is instead on learning how well the model is capturing the interaction between diurnally varying emissions and PBL dynamics, driven by meteorology and surface characteristics. This provides information on possible missing sources in the emission inventories, dominant chemical processes and the impact of the urban heat island (UHI).

We feel that Sect. 3.2 and 3.3 offer different and valuable information on the results using the MEIC Std and MEIC Opt inventories that future urban air quality modelling studies can build on and therefore should retain their current structure.

1510 **8. The title should be placed on the top of the table, as shown in Table 1 on Line 1163. Please correct it in sequence.**

As suggested by the reviewer, each table caption has been placed above the table.

1515 **9. How to modify the PBL stability parameters should be detailed in Sect. 2.1.2 rather than just in results, and should be referenced with the conclusion.**

We agree and have added further details describing the methodology for adjusting the PBL stability parameters. On Page 5 Line 191-195 of the updated manuscript:

1520 *“To account for this, a constant rate of decrease of  $PBLH/L_{MO}$  has been assumed between original modelled values for 3 pm and 8 pm, producing the modified campaign period mean  $PBLH/L_{MO}$  diurnal profile illustrated in Fig. 2. Modified  $L_{MO}$  values from 4-7 pm are added to the set of input meteorological variables for all subsequent simulations, with the directly input  $PBLH$  measurements remaining unchanged.”*

A reference to this description has been added to Page 16 Line 637: *“The early evening stability adjustment (Sect. 2.1.2)...”*

1525 **10. Note some details to the format of the paper. Such as: Please change the font in formula 4 into L into italics. The last name in the legend in Fig 1. is incomplete. The “:” and “.” behind Fig 1. and Fig 2. should be consistent.**

For Fig 1. we have not altered the “Beijing Capital International Airport” label but have instead removed the “meteorology observatory” label in the caption. We have made the other formatting edits as suggested by the reviewer.

1530 **11. Line 560 “The corresponding Fb value improvement, at urban sites, from.....” It should tell the**  
1535 **reader more clearly how the Fb can reflect the traffic emission (for different range)? And some**  
**references should be cited.**

We thank the reviewer for this comment and have further explained how Fb improvement is related to the inclusion of explicitly represented traffic sources through reference to the concentration gradients presented in Fig. 4. Two other ADMS-Urban studies are cited (Dédelé and Miskinyté, 2015; Hood et al. 2018) in which Fb improvements are associated with enhanced traffic emissions from explicit road sources.

Page 15 Line 579-584 of the updated manuscript now reads:

1540 *“This modelled urban NO<sub>2</sub> concentration increase results in a Fb value improvement from -0.13 to 0 (Table 5) reflecting the greater NO<sub>2</sub> levels simulated by the model at locations in close proximity to explicit roads. By using grid sources only, the road traffic emissions are diluted over each 3 x 3 km grid cell and the strong concentration gradients associated with a region densely populated by major roads, illustrated in Fig. 4, are not captured. Similarly, Dédelé and Miskinyté (2015) and Hood et al. (2018) found that increased traffic emissions due to higher traffic volume and adjusted emission factors, respectively, produced improved Fb values using ADMS-Urban.”*

1545 **12. Line 570: “Little change is seen across suburban areas with the inclusion of explicit road source emissions, reflecting the lower density of roads and more dominant contribution from diffuse emissions with distance away from Beijing’s urban centre”. Please make more explanation.**

We have included additional references to model evaluation statistics (Line 593) in order to emphasise the lack of influence of explicit road sources on suburban NO<sub>2</sub> concentrations compared with urban locations. The strong concentration gradients influencing near-road urban locations are not present across suburban areas, with diffuse emissions from residential sources having a stronger influence. Two studies investigating the importance of residential heating and cooking emissions from coal combustion in Beijing are now cited (Cai et al. 2018; Li et al. 2018).

Page 15 Line 593-599 of the updated manuscript now reads:

1555 *“Minimal R value changes and a much lower Fb improvement, from -0.03 to 0.02, are seen across suburban compared to urban areas, following the inclusion of explicit road source emissions. This reflects the lower density of roads in suburban areas (Fig. 4) and therefore absence of the strong concentration gradients that enhance NO<sub>2</sub> levels at near-road urban locations. The relative influence of diffuse emissions contained within the underlying gridded emission sources on simulated pollutant concentrations is therefore more prominent with distance from Beijing’s urban centre, with previous studies specifically highlighting the persisting importance of residential coal combustion for heating and cooking during winter in suburban and rural Beijing (Cai et al. 2018, Li et al. 2018).”*

1565 **13. Line 620: “The results suggest that although atmospheric stability has a strong impact on NO<sub>2</sub> concentrations, the use of observed PBLH instead of modelled heights has little effect”. This conclusion should be extended.**

This conclusion has been extended to more clearly highlight the small impact of PBLH changes on NO<sub>2</sub> concentrations, during the parts of the day when stability is unchanged, compared with the large NO<sub>2</sub> level decrease (~ 15 µg m<sup>-3</sup>) at 4 pm for the simulations in which measured PBLH is used with and without the stability correction.

1570 Page 17 Lines 648-654: *“This is clearest outside the hours in which the stability correction has been applied, when large (~300 µg m<sup>-3</sup>) measured and modelled mid-afternoon and nighttime PBLH discrepancies have negligible impact on simulated NO<sub>2</sub> concentrations. The greater impact of PBL stability changes alone, however, is clearly evidenced by the ~15 µg m<sup>-3</sup> difference at 4 pm between simulations using measured PBLHs with and*

1575 *without the stability correction. This dominant influence of PBL stability is possibly related to the impact in the model configuration of near-surface traffic emissions and the exclusion of elevated point sources, with pollution dispersion from the latter more likely to be restricted by low PBLHs which would then further affect modelled NO<sub>2</sub> levels.”*

**Referee #2**

1580 **In this paper, Biggart et al presented a street-level air quality simulation study for Beijing urban area using an urban air pollution dispersion and chemistry model ADMS-Urban. The predictions were evaluated against observations during winter campaign in 2016 in the same area. Several sensitivity tests were conducted to investigate possible reasons for the discrepancies between model and observations. Studies like this provide useful information on high-resolution air quality simulation in complex urban areas. The paper is generally well written. A few comments are provided below:**

1585 We thank the reviewer for their positive feedback.

1. **The model domain for ADMS-Urban is 75 km x 90 km. Author mentioned that the model has street-level resolution, what is the exact resolution setting in the model in terms of metres? Does the resolution vary between different land uses, eg. Road and other areas? If they all use the same resolution as road, then it would require a very high computational demand.**

1590 We thank the reviewer for this comment and highlighting our need to precisely define ‘street-level’ resolution.

The reviewer is also correct to query whether the model resolution varies across the domain. To clarify, the pollutant concentration maps presented in Fig. 4 have been generated with both a regular grid of output points at ~150 m resolution as well as an array of receptor points added within and in the immediate vicinity of all individual road emission source segments. The additional receptor points increases the model resolution to < 10 m in regions containing dense distributions of explicit road sources, therefore enabling the sharp pollutant concentration variations adjacent to roads to be captured.

1600 In Sections 3.2-3.7 modelled concentrations are compared with measurements recorded at monitoring network stations and the IAP field campaign site. For this work, as stated in Sect. 2.3 Line 308, modelled concentrations are output at exact locations by defining the coordinates of the measurement points in the model set-up. The computational demand of such simulations in which concentrations are output at a small number of locations is substantially lower than that required to produce the fully resolved maps in Fig. 4.

The manuscript has been altered to clarify the resolution of the concentration maps presented in Sect. 3.1. Page 9 Line 326-332 of the updated manuscript:

1605 *“In this study, the statistical evaluation of pollutant concentrations simulated at the exact coordinates of the measurement locations is complemented by street-scale resolution maps which more clearly illustrate the strong spatial heterogeneity of pollution levels across Beijing. Fully resolved PM<sub>2.5</sub>, NO<sub>2</sub> and O<sub>3</sub> concentration fields in central Beijing are simulated with a combination of regularly spaced receptor points at ~150 m and additional output points distributed within and in the immediate vicinity of all individual road emission source segments. The addition of emission source-oriented output points increases the model resolution to < 10 m across regions containing dense distributions of explicit road sources, therefore enabling the sharp pollutant concentration variations adjacent to roads to be captured.”*

2. **Page 6 Line 225 “Measured concentrations at 12 of the 35 monitoring stations in Beijing were used to produce the background concentration.” Is there a specific reason to exclude the other 23 stations?**

1615 This is an important point raised by the reviewer. We have used measurement data from the 12 stations in Beijing that are part of the national monitoring network run by the CNEMC. The remaining 23 stations making up the

full network in Beijing were run by a different organisation and therefore may be subject to different data quality control procedures. Measurements from the 12 national stations we provided to all APHH-China participants. The manuscript has been updated to make this clearer, Page 6 Line 230-233 now reads:

1620 “Measured concentrations at 12 national air quality monitoring stations, run by the China National Environmental  
Monitoring Center (CNEMC), the IAP field site and an additional site 60 km SE of Beijing, situated in the built-  
up Guangyang district of Langfang in Hebei province, are used to estimate this background concentration field.”

**3. Page 7 Line 245, agricultural emissions not included in the model simulation?**

This is correct. The standard available (<http://www.meicmodel.org/>) MEIC v1.3 emissions include transportation,  
1625 power, industry, residential and agricultural sectors. However, the 3 km MEIC emissions covering urban and  
suburban Beijing, provided by our APHH-China collaborators at Tsinghua University, exclude the agricultural  
sector. This is reasonable owing to the negligible amount of agriculture within our modelling domain. We have  
added this caveat to Page 7 Line 250 of the manuscript to clarify the omission of agricultural emissions:

1630 *“Note that the latter is not used in this study due to both the lack of farmland in urban Beijing and the negligible  
contributions to the pollutant species simulated in this study from agricultural emission sources (Qi et al. 2017).”*

**4. Page 7 Line 250, emissions for the industrial and residential sectors were distributed based on  
Gross Domestic Product (GDP) and population density to grid-level resolution? What’s the  
resolution for this? Is information of GDP and population density available at your grid level  
resolutions?**

1635 The industrial and residential source sectors (plus non-road transportation) in the MEIC emissions inventory,  
developed by Tsinghua University, were initially calculated at the provincial spatial scale using provincial level  
activity data (e.g energy consumption, fuel type, manufacturing technology, air pollution control devices) and  
emission factors. This information is largely unpublished but was collected by the MEIC development group  
from a range of databases (e.g Chinese Environmental Statistics, China’s Pollution Source Census, China Energy  
1640 Statistical Yearbook) (Qi et al. 2017). Emissions calculated for each province are then downscaled to county level  
and then to grid-scales of different resolutions using spatial proxies. County-level GDP, published in the China  
Statistical Yearbook by the National Bureau of Statistics ([www.data.stats.gov.cn](http://www.data.stats.gov.cn)), and urban population are used  
for the industrial sector, with urban population and rural population used for the residential sector (Zheng et al.  
2017). The population density data used for MEIC was generated by the Oak Ridge National Laboratory with the  
1645 LandScan global population distribution model which generates global population distribution data at resolutions  
up to ~1 km (available for free download from [www.landscan.ornl.gov](http://www.landscan.ornl.gov)). The MEIC emission inventory is  
produced by allocating emissions using the ~1 km resolution proxy data before aggregating to the coarser 3 km x  
3 km resolution emissions used for this study (Qi et al. 2017).

The manuscript has been updated Page 7 Line 256-260:

1650 *“Industrial and residential sector emissions are calculated from provincial level activity data and emission  
factors (Zheng et al. 2017). Industrial emissions are then downscaled to the county level using GDP (National  
Bureau of Statistics, 2014), with both industry and residential emissions further distributed to grid level  
resolutions based on high resolution (~1 km) population density data (Oak Ridge National Laboratory, 2013)  
(Zheng et al. 2017).”*

**5. Table 3 provides the weighting factors for road emissions. Are the weighting factors the same for  
all pollutants that simulated in this study?**

We thank the reviewer for this comment. Yes, the weighting factors provided in Table 3 are the same for all  
simulated pollutant species. In this study, the weighting factors for the allocation of gridded transportation  
emissions to individual road segments act as proxies for traffic volume (described on page 8 Line 290). For  
1660 instance, motorways (weighting factor = 0.7) are expected to have substantially higher traffic volume than

tertiary roads (weighting factor = 0.15). Further adjusting road emissions weighting factors for pollutant type would imply that the vehicle fleet composition on each road type is substantially different with different vehicle categories manufactured to varying emission standards resulting in some vehicles producing stronger or weaker emissions of particular pollutants than others. This may be an important consideration in Beijing due to, for instance, the strong temporal variation in location and volume of heavy duty diesel trucks (HDDTs). As discussed on Page 12 Line 452, HDDTs which often originate in provinces with less stringent emission standards flood into central Beijing at night following their daytime restrictions. Therefore, future work accounting for traffic volume, speed and composition variations on different road types would certainly be valuable but is outside the scope of this study.

1665

1670 We have added the following text to the updated manuscript. Page 8 Line 293: of the updated manuscript:

*"Each road type weighting factor is applied equally to all pollutant species."*

Line 296:

*"...This methodology is based on the assumption that traffic volume, speed and fleet composition are constant across all road type classes listed in Table 3."*

1675 Line 301:

*"Additionally, Zhang et al. (2018) observed a greater proportion of vehicles with lower emission standards on roads outside the Fifth Ring Road."*

**6. Page 8 Line 290, the urban areas are more congested than suburban. This study used the same weightings factors for urban and suburban, which may underestimate the urban emissions. It is recommended to try different weighting factors for urban and suburban and test the impacts on simulation results.**

1680

We thank the reviewer for this suggestion. As we explain on Page 8 Line 297, substantial variations in traffic volume and speed with distance from Beijing's urban centre have previously been observed (Jing et al. 2016). However, this is largely accounted for by the underlying gridded transport sector emissions that are downscaled to grid level resolution using road network and vehicle kilometres travelled data (Zheng et al. 2014), producing a generally decreasing magnitude of transport emissions towards suburban Beijing. The application of different weighting factors on urban and suburban roads would imply that the greater congestion levels in urban areas results in, for example, a higher proportion of total traffic on primary versus tertiary roads compared to suburban areas. This seems like a reasonable hypothesis, however similarly to the previous suggestion to change weighting factors for different pollutants, reproducing the explicit traffic emissions inventory with varied weightings between urban and suburban areas and repeating simulations would require considerable extra computational effort than available. Adjusting weighting factors for pollutant type and urban/suburban areas would be interesting sensitivity studies for future work aiming to refine the production of explicit road emissions networks in urban areas where data-intensive bottom-up methodologies are not possible.

1690

1695

A sentence has been added to the manuscript (Sect. 4 Page 17 Line 676-679) to summarise the potential benefits of incorporating weighting factor variations:

*"Future work could focus on refining the explicit road emissions network created here by testing the impact of adjusting weighting factors for different pollutants and across urban and suburban areas to better account for the impact of traffic congestion and vehicle type, such as HDDTs, on emissions along different road classifications."*

1700

**7. Figure 16: suggest to change the color scheme for "Grids & Roads" and "Grid only". It is very hard to distinguish them on the map.**

Thank you. The “Grids only” simulation results are now plotted in orange, with “Grids and Roads” in blue.

1705

## References

Cai, H., and Xie, S.: Traffic-related air pollution modelling during the 2008 Beijing Olympic Games: The effects of an odd-even day traffic restriction scheme, *Science of The Total Environment*, 408, 1935-1948, <https://doi.org/10.1016/j.scitotenv.2011.01.025>, 2011.

1710 Cai, S., Li, Q., Wang, S., Chen, J., Ding, D., Zhao, B., Yang, D., Hao, J.: Pollutant emissions from residential combustion and reduction strategies estimated via a village-based emission inventory in Beijing, *Environ. Poll.*, 238, 230-237, <https://doi.org/10.1016/j.envpol.2018.03.036>, 2018.

Carruthers, D. J.: airTEXT air quality forecasting system, Towards eEnvironment, GMES meeting, Prague, Czech Republic, 2009.

1715 Chang, X., Wang, S., Zhao, B., Xing, J., Liu, X., Wei, L., Song, Y., Wu, W., Cai, S., Zheng, H., Ding, D., Zheng, M.: Contributions of inter-city and regional transport to PM<sub>2.5</sub> concentrations in the Beijing-Tianjin-Hebei region and its implications on regional joint air pollution, *Science of The Total Environment*, 660, 1191-1200, <https://doi.org/10.1016/j.scitotenv.2018.12.474>, 2019.

1720 Cheng, J., Su, J., Cui, T., Li, X., Dong, X., Sun, F., Yang, Y., Tong, D., Zheng, Y., Li, J., Zhang, Q., He, K.: Dominant role of emission reduction in PM<sub>2.5</sub> air quality improvement in Beijing during 2013-2017: a model-based decomposition analysis, *Atmos. Chem. Phys.*, <https://doi.org/10.5194/acp-19-6125-2019>, 2019.

Cui, J., Lang, J., Chen, T., Mao, S., Cheng, S., Wang, Z., Cheng, N.: A framework for investigating the air quality variation characteristics based on the monitoring data: Case study for Beijing during 2013-2016, *J. Env. Sci.*, 81, 225-237, <https://doi.org/10.1016/j.jes.2019.01.009>, 2019.

1725 Dédelé, A., Miskinyté, A.: The statistical evaluation and comparison of ADMS-Urban model for the prediction of nitrogen dioxide with air quality monitoring network, *Environ. Monit. Assess.*, 187, <https://doi.org/10.1007/s10661-015-4810-1>, 2015.

1730 Hood, C., MacKenzie, I., Stocker, J., Johnson, K., Carruthers, D., Vieno, M., Doherty, R.: Air quality simulations for London using a coupled regional-to-local modelling system, *Atmos. Chem. Phys.*, 18, 11221-11245, <https://doi.org/10.5194/acp-18-11221-2018>, 2018.

Jing, B., Wu, L., Mao, H., Gong, S., He, J., Zou, C., Song, G., Li, X., Wu, Z.: Development of a vehicle emission inventory with high temporal-spatial resolution based on NRT traffic data and its impact on air pollution in Beijing – Part 1: Development and evaluation of vehicle emission inventory, *Atmos. Chem. Phys.*, 16, 3161-3170, doi:10.5194/acp-16-3161-2016, 2016.

1735 Li, J., Du, H., Wang, Z., Sun, Y., Yang, W., Li, J., Tang, X., Fu, P.: Rapid formation of a severe regional winter haze episode over a mega-city cluster on the North China Plain, *Environ. Poll.*, 223, 605-615, <https://doi.org/10.1016/j.envpol.2017.01.063>, 2017.

1740 Li, X., Wu, J., Elser, M., Feng, T., Cao, J., El-Haddad, I., Huang, R., Tie, X., Prévot, A. S. H., Li, G.: Contributions of residential coal combustion to the air quality in Beijing-Tianjin-Hebei (BTH), China: a case study, *Atmos. Chem. Phys.*, 18, 10675-10691, <https://doi.org/10.5194/acp-18-10675-2018>, 2018.

Liu, L., Huang, X., Ding, A., Fu, C.: Dust-induced radiative feedbacks in north China: A dust storm episode modelling study using WRF-Chem, *Atmos. Environ.*, 129, 43-54, <https://doi.org/10.1016/j.atmosenv.2016.01.019>, 2016.

- 1745 Lugon, L., Sartelet, K., Kim, Y., Vigneron, J., Chrétien, O.: Street-in-Grid modeling of gas-phase pollutants in Paris city, *Atmos. Chem. Phys. Discuss.*, <https://doi.org/10.5194/acp-2019-1087>, in review, 2019.
- McHugh, C. A., Sheng, X., Carruthers, D. J.: Using ADMS models for air quality assessment and management in China, *Chinese Journal of Population Resources and Environment*, 3, 2005.
- Ni, Z., Luo, K., Gao, Y., Gao, X., Fan, J., Cen, K.: Potential air quality improvements from ultralow emissions at coal-fired power plants in China, *Aerosol and Air Quality Research*, 18, 1944-1951, doi: 10.4209/aaqr.2018.02.0070, 2018.
- 1750 Petaja, T., Jarvi, L., Kerminen, V.-M., Ding, A. J., Sun, J. N., Nie, W., Kujansuu, J., Virkkula, A., Yang, X., Fu, C. B., Zilitinkevich, S., Kulmala, M.: Enhanced air pollution via aerosol-boundary layer feedback in China, *Scientific Reports*, 6, DOI: 10.1038/srep18998, 2016.
- Qi, J., Zheng, B., Li, M., Yu, F., Chen, C., Liu, F., Zhou, X., Yuan, J., Zhang, Q., He, K.: A high-resolution air pollutants emission inventory in 2013 for the Beijing-Tianjin-Hebei region, China, *Atmos. Environ.*, 170, 156-168, <https://doi.org/10.1016/j.atmosenv.2017.09.039>, 2017.
- 1755 Sun, W., Shao, M., Granier, C., Liu, Y., Ye, C. S., Zheng, J. Y.: Long-term trends of anthropogenic SO<sub>2</sub>, NO<sub>x</sub>, CO, and NMVOCs emissions in China, *Earth's Future*, 6, 1112-1133 <https://doi.org/10.1029/2018EF000822>, 2018.
- 1760 Wang, Y., Bao, S., Wang, S., Hu, Y., Shi, X., Wang, J., Zhao, B., Jiang, J., Zheng, M., Wu, M., Russell, A. G., Wang, Y., and Hao, J.: Local and regional contributions to fine particulate matter in Beijing during heavy haze episodes, *Science of The Total Environment*, 580, 283-296, <https://doi.org/10.1016/j.scitotenv.2016.12.127>, 2017.
- Wang, H., Peng, Y., Zhang, X., Liu, H., Zhang, M., Che, H., Cheng, Y., Zheng, Y.: Contributions to the explosive growth of PM<sub>2.5</sub> mass due to aerosol-radiation feedback and decrease in turbulent diffusion during a red alert heavy haze in Beijing-Tianjin-Hebei, China, *Atmos. Chem. Phys.*, 18, 17717-17733, <https://doi.org/10.5194/acp-18-17717-2018>, 2018.
- 1765 Wang, N., Lyu, X., Deng, X., Huang, X., Jiang, F., Ding, A.: Aggravating O<sub>3</sub> pollution due to NO<sub>x</sub> emission control in eastern China, *Science of The Total Environment*, 677, 732-744, <https://doi.org/10.1016/j.scitotenv.2019.04.388>, 2019.
- 1770 Xu, J., Yang, W., Han, B., Wang, M., Wang, Z., Zhao, Z., Bai, Z., Vedel, S.: An advanced spatio-temporal model for particulate matter and gaseous pollutants in Beijing, China, *Atmos. Env.*, 211, 120-127, <https://doi.org/10.1016/j.atmosenv.2019.04.011>, 2019.
- Xu, M., Sbihi, H., Pan, X., Brauer, M.: Local variation of PM<sub>2.5</sub> and NO<sub>2</sub> concentrations within metropolitan Beijing, *Atmos. Env.*, 200, 254-263, <https://doi.org/10.1016/j.atmosenv.2018.12.014>, 2019.
- 1775 Yang, D., Zhang, S., Niu, T., Wang, Y., Xu, H., Zhang, K. M., Wu, Y.: High-resolution mapping of vehicle emissions of atmospheric pollutants based on large-scale, real-world traffic datasets, *Atmos. Chem. Phys. Discuss.*, <https://doi.org/10.5194/acp-2019-32>, 2019.
- Zhang, Y., Andre, M., Liu, Y., Wu, L., Jing, B., Mao, H.: Evaluation of low emission zone policy on vehicle emission reduction in Beijing, China, *IOP Conf. Ser.: Earth Environ. Sci.*, 121, doi :10.1088/1755-1315/121/5/0520702018, 2018.
- 1780 Zheng, B., Zhang, Q., Tong, D., Chen, C., Hong, C., Li, M., Geng, G., Lei, Y., Huo, H., He, K.: Resolution dependence of uncertainties in gridded emission inventories: a case study in Hebei, China, *Atmos. Chem. Phys.*, 17 921-933, doi:10.5194/acp-17-921-2017, 2017.

1785

1790

1795

1800

1805

1810

